THE LUMINOSITY FUNCTION OF GALAXIES IN THE LAS CAMPANAS REDSHIFT SURVEY

HUAN LIN[1] AND ROBERT P. KIRSHNER
Harvard-Smithsonian Center for Astrophysics, 60 Garden Street, Cambridge, MA 02138;
hlin@cfa.harvard.edu, kirshner@cfa.harvard.edu

STEPHEN A. SHECTMAN AND STEPHEN D. LANDY
Carnegie Observatories, 813 Santa Barbara Street, Pasadena, CA 91101; shec@ociw.edu, landy@ociw.edu

AUGUSTUS OEMLER
Department of Astronomy, Yale University, New Haven, CT 06520-8101; oemler@astro.yale.edu

DOUGLAS L. TUCKER
Astrophysikalisches Institut Potsdam, An der Sternwarte 16, D-14482 Potsdam, Germany; dtucker@aip.de

AND

PAUL L. SCHECHTER
Department of Physics, Massachusetts Institute of Technology, Cambridge, MA 02139; schech@achernar.mit.edu

ABSTRACT

We present the r-band luminosity function for a sample of 18,678 galaxies, with average redshift $z = 0.1$, from the Las Campanas Redshift Survey (LCRS). The luminosity function may be fitted by a Schechter function with $M^* = -20.29 \pm 0.02 + 5 \log h$, $\alpha = -0.70 \pm 0.05$, and $\phi^* = 0.019 \pm 0.001$ h^3 Mpc^{-3}, for absolute magnitudes $-23.0 \leq M - 5 \log h \leq -17.5$ and $h = H_0/(100$ km s^{-1} Mpc$^{-1})$. Over the same absolute magnitude range, the mean galaxy density is 0.029 ± 0.002 h^3 Mpc^{-3} for a volume extending to $cz = 60,000$ km s^{-1}.

We compare our luminosity function to that from other redshift surveys; in particular, our luminosity function normalization is consistent with that of the Stromlo-APM survey and is therefore a factor of 2 below the normalization implied by the $b_J \approx 20$ bright galaxy counts. Our normalization thus indicates that much more evolution is needed to match the faint galaxy count data, compared to minimal evolution models that normalize at $b_J \approx 20$. Also, we show that our faint-end slope $\alpha = -0.7$, though "shallower" than typical previous values $\alpha = -1$, results primarily from fitting the detailed shape of the LCRS luminosity function, rather than from any absence of intrinsically faint galaxies from our survey.

Finally, we find that the faint end of the luminosity function is dominated by galaxies with emission lines. Using [O II] $\lambda 3727$ equivalent width $W_\lambda = 5$ Å as the dividing line, we find significant differences in the luminosity functions of emission and nonemission galaxies, particularly in their α values; emission galaxies have Schechter parameters $M^* = -20.03 \pm 0.03 + 5 \log h$ and $\alpha = -0.9 \pm 0.1$, while nonemission galaxies are described by $M^* = -20.22 \pm 0.02 + 5 \log h$ and $\alpha = -0.3 \pm 0.1$. The average [O II] $\lambda 3727$ equivalent widths do not change significantly with redshift, consistent with a star formation rate that stays constant over the depths sampled by the LCRS. This result holds for galaxies of different luminosities and over the respective redshift ranges that these galaxies may be observed, in particular up to about $z = 0.2$ for galaxies brighter than M^*.

Subject headings: cosmology: observations — galaxies: distances and redshifts —
galaxies: luminosity function, mass function — surveys

1. INTRODUCTION

The galaxy luminosity function is one of the most basic and fundamentally important quantities in observational cosmology. For example, it is essential for the analysis of large-scale structure statistics from redshift surveys, and knowledge of the local luminosity function is necessary for the proper interpretation of the faint galaxy count data and galaxy evolution at high redshift (e.g., Koo & Kron 1992).

Though much work has gone into determination of the local $z = 0$ optical luminosity function (see Felten 1977; Kirshner, Oemler, & Schechter 1979; Kirshner et al. 1983; Efstathiou et al. 1988; Binggeli, Sandage, & Tammann 1988; and recent work by Loveday et al. 1992; Marzke, Huchra, & Geller 1994b), there is still some uncertainty in its faint end as well as in its normalization (see, e.g., Colless 1995). In this paper we investigate the local luminosity function by presenting results for a sample of 18,678 Las Campanas Redshift Survey (LCRS) galaxies, selected from CCD photometry in a "hybrid" red Kron-Cousins R-band (see § 2 below). This is the largest galaxy sample for which the luminosity function and mean density have been computed. The combination of the mean survey depth of $z = 0.1$ and the large survey volume (1.0×10^7 h^{-3} Mpc^3 out to $cz = 60,000$ km s^{-1}) imply that our results are not biased by local inhomogeneities. In addition, the spectra of LCRS

---

[1] Present affiliation: Department of Astronomy, University of Toronto, 60 St. George Street, Toronto, ONT M5S 3H8, Canada; lin@astro.utoronto.ca.

galaxies allow us to study the luminosity function for samples divided by [O II] $\lambda 3727$ emission strength, a rough indicator of the star formation rate (Kennicutt 1992).

We describe relevant aspects of the LCRS construction in § 2. We then detail our methods for measuring the galaxy luminosity function and mean density in § 3. Our results are presented in § 4, and we compare them to those of other redshift surveys in § 5. Some implications of our results for faint galaxy counts and galaxy evolution are discussed in § 6. We summarize our conclusions in § 7.

2. THE LAS CAMPANAS SURVEY DATA

We begin by describing the Las Campanas survey parameters; detailed descriptions of the LCRS may be found in Shectman et al. (1992, 1995, 1996), Tucker (1994), and Lin (1995). There are 23,690 galaxies, with an average redshift $z = 0.1$, that lie within the survey photometric limits and geometric borders considered in this paper. The survey galaxies were selected from drift scans taken on the Las Campanas 1.0 m Swope telescope with a Gunn r filter (Thuan & Gunn 1976). Follow-up spectroscopy was obtained using the multiobject fiber-optic spectrograph on the Las Campanas 2.5 m DuPont telescope. The survey geometry is that of six " slices," $1\overset{\circ}{.}5$ in declination by $80°$ in right ascension, three each in the North and South galactic caps.

The survey data may be divided into two main parts: the first 20% of the data was obtained using a 50 object fiber system, while the remaining 80% of the data was taken with a 112 object system. The survey slices were built up by observing $1\overset{\circ}{.}5$ by $1\overset{\circ}{.}5$ spectroscopic fields, with a maximum of 50 or 112 galaxies observed per field. The survey photometric limits were chosen so that there would be typically more targets per field than available fibers, and we selected targets at random among those that met the selection criteria. Because we generally do not reobserve any of our fields, we keep track of the variable field-to-field sampling fractions f_i in our subsequent statistical analyses.

To be precise, though our photometry was obtained through a Gunn r filter, the calibration was done relative to standard stars (Graham 1981, 1982) in the Kron-Cousins R-band. Our magnitudes are thus in a "hybrid" Kron-Cousins R system. Nevertheless, the difference between our hybrid Kron-Cousins R system and the true one is small; comparison of photometry of LCRS galaxies obtained in both systems yields a zero-point difference of <0.1 mag and a color term of <0.2 mag per magnitude of the color (Johnson V − Kron-Cousins R). See Tucker (1994) and Shectman et al. (1996) for more details.

Objects were selected for the survey using isophotal magnitudes m, applying both faint and bright isophotal magnitude limits. The limiting isophote is 15% of sky, or approximately 23 mag arcsec^{-2}. In addition, a central magnitude m_c, approximately measuring flux that would enter through the $3\overset{''}{.}5$ diameter aperture of a fiber, is also computed for each object. An additional cut line in the m-m_c plane is then imposed in order to exclude low central surface brightness objects, for which redshifts are more difficult to obtain. For the 50 fiber data, the nominal isophotal magnitude limits are $16.0 \le m < 17.3$, and the central surface brightness cut excludes about 20% of objects otherwise meeting the isophotal limits. For the 112 fiber data, the nominal isophotal limits are $15.0 \le m < 17.7$, with exclusion of just the lowest 4%–9% of objects by surface brightness. We illustrate our isophotal and central magnitude selection criteria for a sample of LCRS galaxies in Figure 1. There are small field-to-field variations from the nominal photometric limits; these are accounted for in our analyses. We will find it convenient to divide our data into four subsets by galactic cap, North and South, and by fiber number, 50 and 112 fibers; we will refer to these subsets as N50, S50, N112, and S112. Table 1 summarizes details concerning these four samples. Also, it turns out that our fiducial sample will be the combined North plus South 112-fiber data set, which we will refer to as NS112.

Throughout this paper we adopt a Hubble constant $H_0 = 100\,h$ km s^{-1} Mpc^{-1} and a deceleration parameter $q_0 = 0.5$. Where the h dependence is not explicitly indicated, we have used $h = 1$. We also assume a uniform Hubble flow so that the absolute magnitude M of a galaxy of isophotal magnitude m and redshift z is given by

$$M = m - 25 - 5 \log d_L - k(z) , \tag{1}$$

where the luminosity distance d_L is

$$d_L = \frac{c}{H_0 q_0^2} [q_0 z + (1 - q_0)(1 - \sqrt{1 + 2 q_0 z})] , \tag{2}$$

and where the k-correction $k(z)$ is taken to be

$$k(z) = 2.5 \log (1 + z) , \tag{3}$$

as appropriate in the mean for an r-band–selected galaxy sample (Tucker 1994; Kirshner et al. 1983). Note that galaxy peculiar velocities, of order $\sigma_{12}/2^{1/2} \approx 350$ km s^{-1} (σ_{12} is the *pairwise* peculiar velocity dispersion; see Lin et al. 1996b; Marzke et al. 1995), and our velocity measurement errors, on average 67 km s^{-1} (Lin 1995), are both quite small compared to the mean survey redshift $cz = 30,000$ km s^{-1}. We therefore neglect the effect of peculiar velocities and velocity errors in the calculation of absolute magnitudes. Similarly, the effect of using a different value of q_0 is also small: $M(q_0') - M(q_0 = 0.5) \approx (q_0' - 0.5)z$, e.g., -0.04 mag at our average $z = 0.1$ for the case $q_0' = 0.1$.

3. METHODS

3.1. *Luminosity Function*

We compute the luminosity function using two related methods that are unbiased by density inhomogeneities in the galaxy distribution. These are the parametric maximum-likelihood method of Sandage, Tammann, & Yahil (1979, hereafter STY)
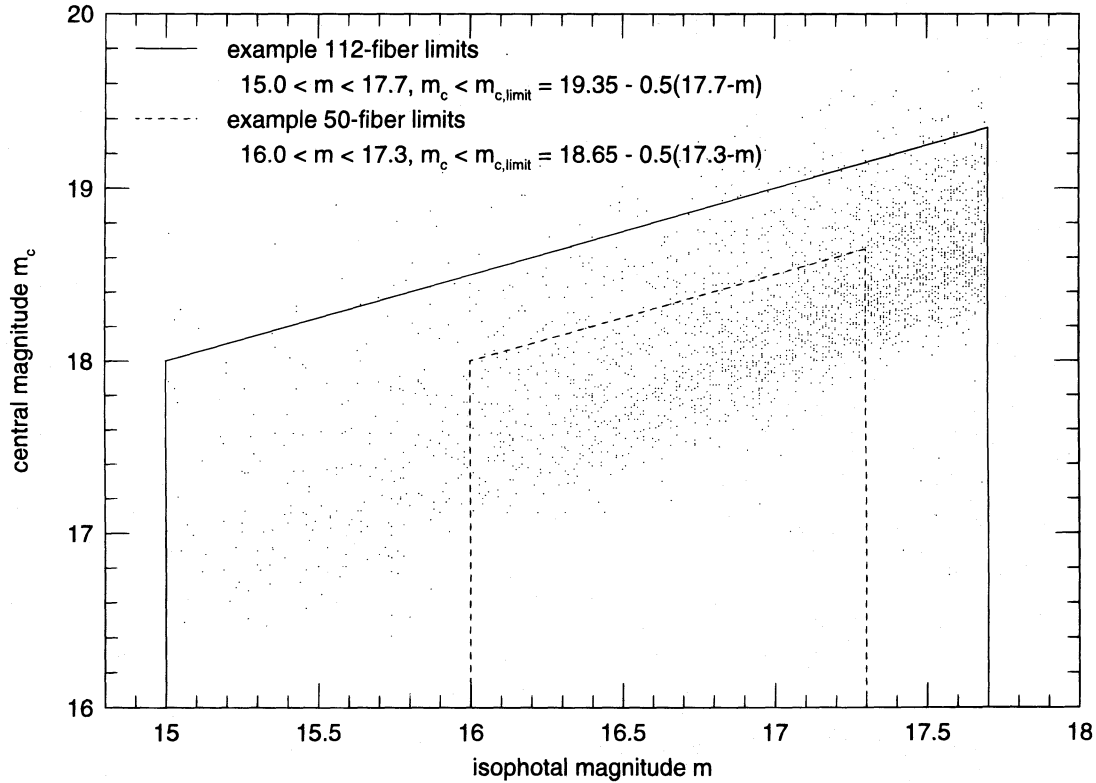
FIG. 1.—Examples of the photometric selection criteria in the isophotal magnitude (m)–central magnitude (m_c) plane applied to the 112- and 50-fiber LCRS data; $-12°$ slice, epoch 1992.3.

and the nonparametric stepwise maximum-likelihood (SWML) method of Efstathiou, Ellis, & Peterson (1988, hereafter EEP). We describe these methods below, and we will discuss some modifications needed in the analysis of the LCRS sample in § 3.2.

Consider a galaxy i observed at redshift z_i in a flux-limited redshift survey like the LCRS. Let $m_{min, i}$ and $m_{max, i}$ denote the apparent magnitude limits of the field in which galaxy i is located. Let $\phi(M)$ be the differential galaxy luminosity function which we want to determine. Then the probability that galaxy i has absolute magnitude M_i is given by

$$p_i \equiv p(M_i \,|\, z_i) = \phi(M_i) \Big/ \int_{M_{min}(z_i)}^{M_{max}(z_i)} \phi(M)dM \;,\tag{4}$$

where the absolute magnitude limits at z_i are

$$\begin{Bmatrix} M_{min}(z_i) \\ M_{max}(z_i) \end{Bmatrix} = \begin{Bmatrix} m_{min, i} \\ m_{max, i} \end{Bmatrix} - 25 - 5 \log d_{Li} - k(z_i) \;.\tag{5}$$

The luminosity distance d_L and the k-correction $k(z)$ for LCRS galaxies are computed as described in § 2. We can then form a likelihood function $\mathscr{L}$ for having a survey of N galaxies, with respective absolute magnitudes M_i, by multiplying the probabilities p_i:

$$\mathscr{L} = p(M_1, \ldots, M_N \,|\, z_1, \ldots, z_N) = \prod_{i=1}^{N} p_i \;,\tag{6}$$

TABLE 1

LCRS SUBSAMPLES

Sample	N [a]	$\bar{f}$ [b]	m_1 [c]	m_2 [c]	Percent LSB [d]
North 50-fiber (N50)	2706	0.66	16.0	17.3	22%
South 50-fiber (S50)	2054	0.50	16.0	17.3	21
North 112-fiber (N112)......	8552	0.71	15.0	17.7	4
South 112-fiber (S112).......	10378	0.69	15.0	17.7	9

[a] Number of galaxies observed which lie within the survey photometric limits and geometric borders.
[b] Mean sampling fraction for galaxies within photometric limits and geometric borders.
[c] Nominal isophotal magnitude limits: $m_1 \leq m < m_2$.
[d] Percentage of objects excluded for low central surface brightness but otherwise within the isophotal limits.

or

$$\ln \mathscr{L} = \sum_{i=1}^{N} \left[\ln \phi(M_i) - \ln \int_{M_{\min}(z_i)}^{M_{\max}(z_i)} \phi(M) dM \right] . \tag{7}$$

In the STY method one assumes a parametric model for $\phi(M)$, and the parameters describing $\phi(M)$ are determined by maximizing the likelihood $\mathscr{L}$, or equivalently $\ln \mathscr{L}$, with respect to those parameters. In our case we take as our model for $\phi(M)$ the Schechter function (Schechter 1976)

$$\phi(M) = (0.4 \ln 10)\phi^*(10^{0.4(M^* - M)})^{1+\alpha} \exp\left(-10^{0.4(M^* - M)}\right) , \tag{8}$$

and use the STY method to find the characteristic magnitude M^* and the faint-end slope α. The normalization ϕ^* drops out in equation (4) and has to be determined using a different method to be described below in § 3.3. Also, error ellipses in the M^*-α plane may be drawn by finding the contour corresponding to

$$\ln \mathscr{L} = \ln \mathscr{L}_{\max} - \tfrac{1}{2}\Delta\chi^2 , \tag{9}$$

where $\Delta\chi^2$ is the change in χ^2 appropriate for the desired confidence level and a χ^2 distribution with 2 degrees of freedom.

Alternatively, one does not have to assume a particular functional form for $\phi(M)$. Rather, in the EEP stepwise maximum-likelihood method (SWML), the luminosity function is taken to be a series of N_p steps, each of width ΔM in absolute magnitude:

$$\phi(M) = \phi_k , \qquad M_k - \Delta M/2 < M < M_k + \Delta M/2 , \qquad k = 1, \dots, N_p . \tag{10}$$

In this case equation (7) may be rewritten as

$$\ln \mathscr{L} = \sum_{i=1}^{N} \sum_{k=1}^{N_p} W(M_i - M_k) \ln \phi_k - \sum_{i=1}^{N} \ln \left\{ \sum_{k=1}^{N_p} \phi_k \Delta M H[M_k, M_{\min}(z_i), M_{\max}(z_i)] \right\} , \tag{11}$$

where the functions W and H are given by

$$W(M_i - M_k) = \begin{cases} 1 , & M_k - \Delta M/2 \le M_i \le M_k + \Delta M/2 \\ 0 , & \text{otherwise} \end{cases} , \tag{12}$$

$H[M_k, M_{\min}(z_i), M_{\max}(z_i)]$

$$= \begin{cases} \min\left[M_k + \Delta M/2, M_{\max}(z_i)\right] - \max\left[M_k - \Delta M/2, M_{\min}(z_i)\right] , & \text{if } M_k + \Delta M/2 \ge M_{\min}(z_i) \text{ and } M_k - \Delta M/2 \le M_{\max}(z_i) \\ 0 , & \text{otherwise} \end{cases} \tag{13}$$

We then maximize $\ln \mathscr{L}$, equation (11), with respect to the parameters ϕ_k, and subsequently solve for them iteratively using

$$\phi_k \Delta M = \left\{ \sum_{i=1}^{N} W(M_i - M_k) \right\} \bigg/ \sum_{i=1}^{N} \left\{ H[M_k, M_{\min}(z_i), M_{\max}(z_i)] \bigg/ \sum_{j=1}^{N_p} \phi_j \Delta M H[M_j, M_{\min}(z_i), M_{\max}(z_i)] \right\} . \tag{14}$$

As in the STY method, the normalization of the ϕ_k is not determined, so we introduce a constraint similar to that given by EEP to fix the normalization:

$$g \equiv \sum_{k=1}^{N_p} \phi_k \Delta M V(M_k)/V(M_f) - 1 = 0 , \tag{15}$$

where $V(M)$ gives the volume (including relativistic effects) over which a galaxy of absolute magnitude M can be seen in a flux-limited survey, and M_f is a fiducial absolute magnitude, which we take to be $-20 \approx M^*$ as appropriate for the LCRS. Also, following EEP, we can estimate the variances of the parameters ϕ_k from the first N_p diagonal elements of the covariance matrix given by

$$\text{cov}(\phi_k) = \mathbf{I}^{-1}(\phi_k) , \tag{16}$$

where $\mathbf{I}(\phi_k)$ is the information matrix

$$\mathbf{I}(\phi_k) = - \left\| \begin{bmatrix} \partial^2 \ln \mathscr{L}/\partial\phi_i \partial\phi_j + (\partial g/\partial\phi_i)(\partial g/\partial\phi_j) & \partial g/\partial\phi_j \\ \partial g/\partial\phi_i & 0 \end{bmatrix} \right\|_{\phi_i, \phi_j = \phi_k} . \tag{17}$$

We can test the goodness of fit of the STY solution by comparing it to the SWML solution using a likelihood ratio test described by EEP. Let $\mathscr{L}_2$ be the likelihood for the SWML solution given by equation (11), and let $\mathscr{L}_1$ be the likelihood, again from equation (11), but with ϕ_k set to $\phi_{\text{STY},k}$, where

$$\phi_{\text{STY},k} = \int_{M_k - \Delta M/2}^{M_k + \Delta M/2} \phi_{\text{STY}}^2(M) V(M) dM \bigg/ \int_{M_k - \Delta M/2}^{M_k + \Delta M/2} \phi_{\text{STY}}(M) V(M) dM . \tag{18}$$

As discussed in EEP, here we use this definition of $\mathcal{L}_1$ for the STY solution, rather than equation (7), in order to match the binning present in equation (11) but absent from equation (7). EEP show that the likelihood ratio $2 \ln(\mathcal{L}_1/\mathcal{L}_2)$ approximately follows a χ^2 distribution with $N_p - 3$ degrees of freedom, giving us a means for testing the quality of the STY solution.

Alternatively, we can also check the goodness of the STY fit by comparing the observed absolute magnitude distribution $dN(M)$ against the distribution $dN_{STY}(M)$ expected from the STY solution and the observed redshift distribution of the N survey galaxies (Yahil et al. 1991):

$$dN_{STY}(M) = \sum_{i=1}^{N} p(M \mid z_i)dM = \sum_{i=1}^{N}\left[\phi(M)dM \Big/ \int_{M_{min}(z_i)}^{M_{max}(z_i)} \phi(M)dM \right]. \tag{19}$$

A χ^2 test can then be used to assess how well the STY prediction matches the observations.

3.2. Modifications

For thoroughness in the analysis of the LCRS data, we need to consider four additional details that will modify the basic methods described above to calculate the luminosity function. The most important effect is that of central surface brightness selection, while the others make fairly small changes in $\phi(M)$.

1. *Magnitude Errors.*—From repeat observations we find that our rms isophotal magnitude error is $\sigma = 0.1$ mag. We make the rough approximation that the magnitude errors are Gaussian distributed with dispersion σ, so that the observed luminosity function ϕ_{obs} is a convolution of the true luminosity function ϕ with a Gaussian magnitude error distribution (EEP). Thus

$$\phi_{obs} = \frac{1}{\sqrt{2\pi}\sigma} \int_{-\infty}^{\infty} \phi(M')e^{-(M'-M)^2/2\sigma^2}dM', \tag{20}$$

and we use ϕ_{obs} in place of ϕ in the parametric STY equations. For simplicity, we will not make this substitution in the nonparametric SWML equations. Accounting for this dispersion of 0.1 mag makes small systematic changes in the best-fit values of the Schechter parameters for our sample: $\Delta M^* \approx +0.03$ and $\Delta\alpha \approx +0.03$.

2. *Variable Field Sampling Fractions.*—To account for this effect, we weight galaxy i's entry in the likelihood equations (7) and (11) by the inverse of the sampling fraction f_i of the field containing that galaxy (Zucca, Pozzetti, & Zamorani 1994):

$$\ln p_i \to \frac{\ln p_i}{f_i}. \tag{21}$$

Including this effect changes the Schechter parameters very little: both $|\Delta M^*|$ and $|\Delta\alpha|$ are < 0.01.

3. *Apparent Magnitude and Surface Brightness Incompletenesses.*—Our success rate in identifying spectra as galaxies and stars drops slightly at fainter apparent magnitudes and also drops slightly close to the limiting central surface brightness cut line (Fig. 1). We define a completeness factor $F(m, m_c - m_{c,limit})$, which is a function of isophotal magnitude m and of "distance" $m_c - m_{c,limit}(m)$ from the central magnitude cut line. We take F to be the fraction of spectra we identified as galaxies or stars in each bin on a grid of m and $m_c - m_{c,limit}(m)$ values. In Figure 2, we plot the two orthogonal projections $F_1(m)$ and $F_2(m_c - m_{c,limit})$ of the full completeness function F for each of the N50, S50, N112, and S112 samples. From the figure we note that the completeness does not vary much with either apparent magnitude or surface brightness; the completeness only drops to about 0.95 at the faint isophotal magnitude limits or at the central surface brightness limits. To account for this effect, we weight galaxy i's entry in the STY and SWML likelihood equations by the inverse of the value of F appropriate for that galaxy's isophotal and central magnitudes:

$$\ln p_i \to \frac{\ln p_i}{F(m_i, m_{ci} - m_{c,limit_i})}. \tag{22}$$

The change introduced is negligible for M^*, $|\Delta M^*| < 0.01$, but α does change systematically by a small amount, $\Delta\alpha \approx -0.04$. (The greater incompleteness at fainter m translates to a bias against intrinsically fainter galaxies and hence a more positive α, if left uncorrected.)

4. *Central Surface Brightness Selection.*—We empirically find in the LCRS a correlation between a galaxy's absolute luminosity and that galaxy's distance from our central surface brightness cut line. We demonstrate this by culling out galaxies from our N112 subset to match the more restrictive surface brightness cuts of the N50/S50 and S112 subsets (§ 2 and Table 1). Figure 3 shows that the effect of the more stringent surface brightness cuts is to reduce the sampling completeness $G(M)$ as the absolute magnitude M becomes fainter, where $G(M)$ is simply the fraction of galaxies at M that remain after the low surface brightness galaxies have been removed. For the N50, S50, and S112 samples, we can account for this bias against faint galaxies by weighting galaxy i's entry in the likelihood equations by the inverse of G at that galaxy's absolute magnitude M_i:

$$\ln p_i \to \frac{\ln p_i}{G(M_i)}. \tag{23}$$

We thus correct the surface brightness sampling of the N50, S50, and S112 subsets to that of the N112 subset. For the 50-fiber data samples, $\Delta M^* \approx -0.04$ and $\Delta\alpha \approx -0.15$; for the S112 sample, $\Delta M^* = -0.01$ and $\Delta\alpha = -0.06$. We do not attempt to extrapolate further and correct for the N112 sample's own central surface brightness cut, though we expect the change to be $|\Delta\alpha| < 0.1$ from the example of the S112 data set.
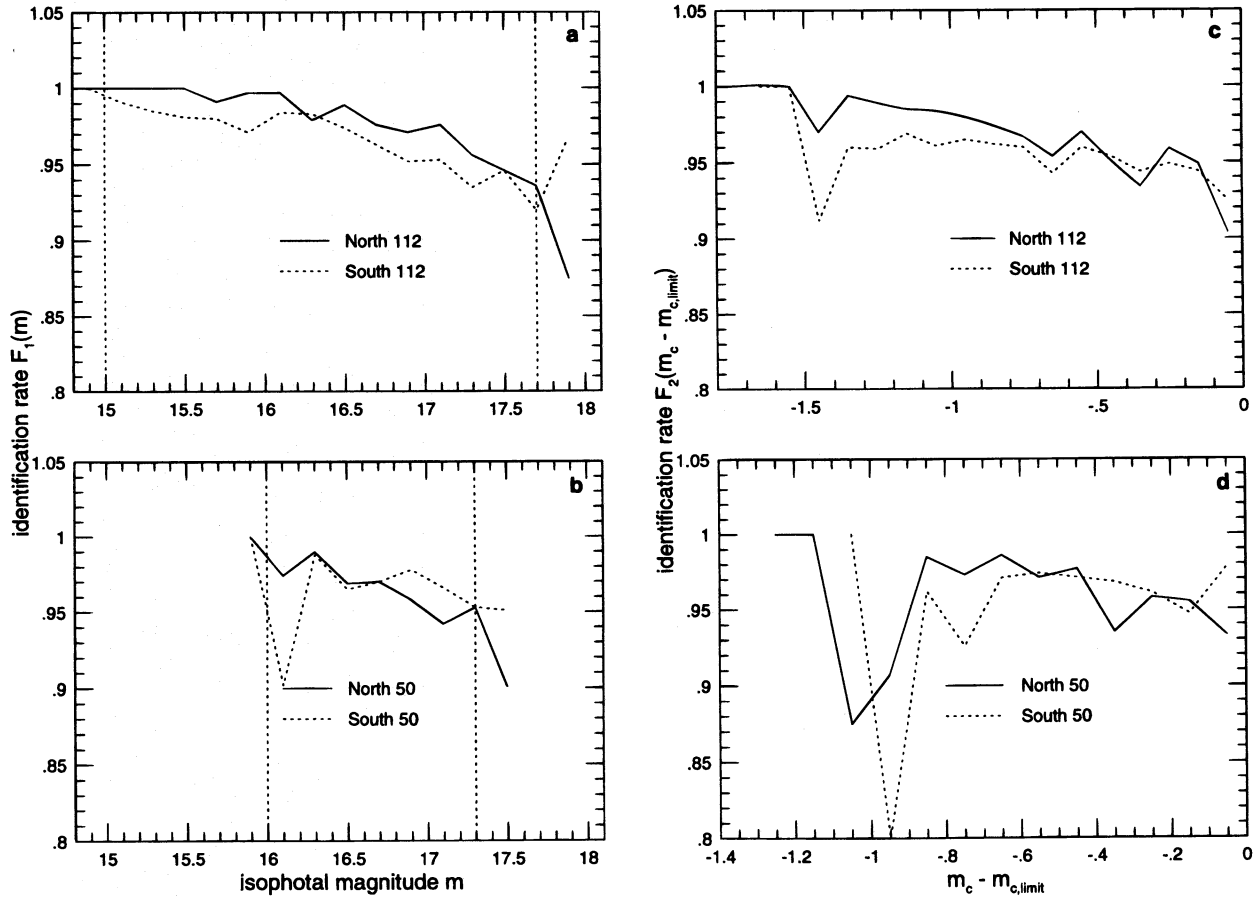
FIG. 2.—(a–b) Identification rate (galaxies plus stars) $F_1(m)$ as a function of apparent magnitude m for the four main subsets of LCRS data. Vertical lines show the nominal isophotal magnitude limits. (c–d) The identification rate $F_2(m_c - m_{c,\text{limit}})$ as a function of "distance" $m_c - m_{c,\text{limit}}$ from the central magnitude limit.

We take account of the latter three effects (2)–(4) together by the replacement

$$\ln p_i \rightarrow W_i \ln p_i, \quad W_i \equiv \frac{1}{f_i F(m_i, m_{ci} - m_{c,\text{limit}_i}) G(M_i)}, \tag{24}$$

that is, we weight by the inverse of the product of the three completeness factors. However, because the weighting factors W_i are greater than 1, the likelihood $\ln \mathscr{L}$ will be larger in absolute value than when no weightings are applied. The likelihood will thus resemble that of a larger sample, leading to systematic underestimates in the confidence ellipses and errors we compute (Glazebrook et al. 1995c). To remedy this, we renormalize the weights W_i so that $\sum_{i=1}^{N} W_i = N$, where N is the number of galaxies in the sample of interest. The original weights are multiplied by renormalization factors of 0.4–0.7 depending on the data set, in particular by 0.68 in the case of our fiducial NS112 sample. We have verified that this procedure yields error estimates similar to those for the case when no weights are applied.

3.3. Mean Density

To calculate the mean galaxy density $\bar{\rho}$, one can use the minimum-variance estimator of Davis & Huchra (1982) (also Loveday et al. 1992). We can adapt it to the LCRS as follows. For galaxies i within redshift limits $z_1 < z_i < z_2$ and absolute magnitude limits $M_1 < M_i < M_2$, we have

$$\bar{\rho} = \frac{\sum_i w(z_i) W_i}{\int_{z_1}^{z_2} S(z) w(z) (dV/dz) dz}, \tag{25}$$

where $S(z)$ is the selection function

$$S(z) = \int_{\max [M_{\min}(z), M_1]}^{\min [M_{\max}(z), M_2]} \phi_{\text{obs}}(M) dM \bigg/ \int_{M_1}^{M_2} \phi(M) dM, \tag{26}$$

and $w(z)$ is the weight function

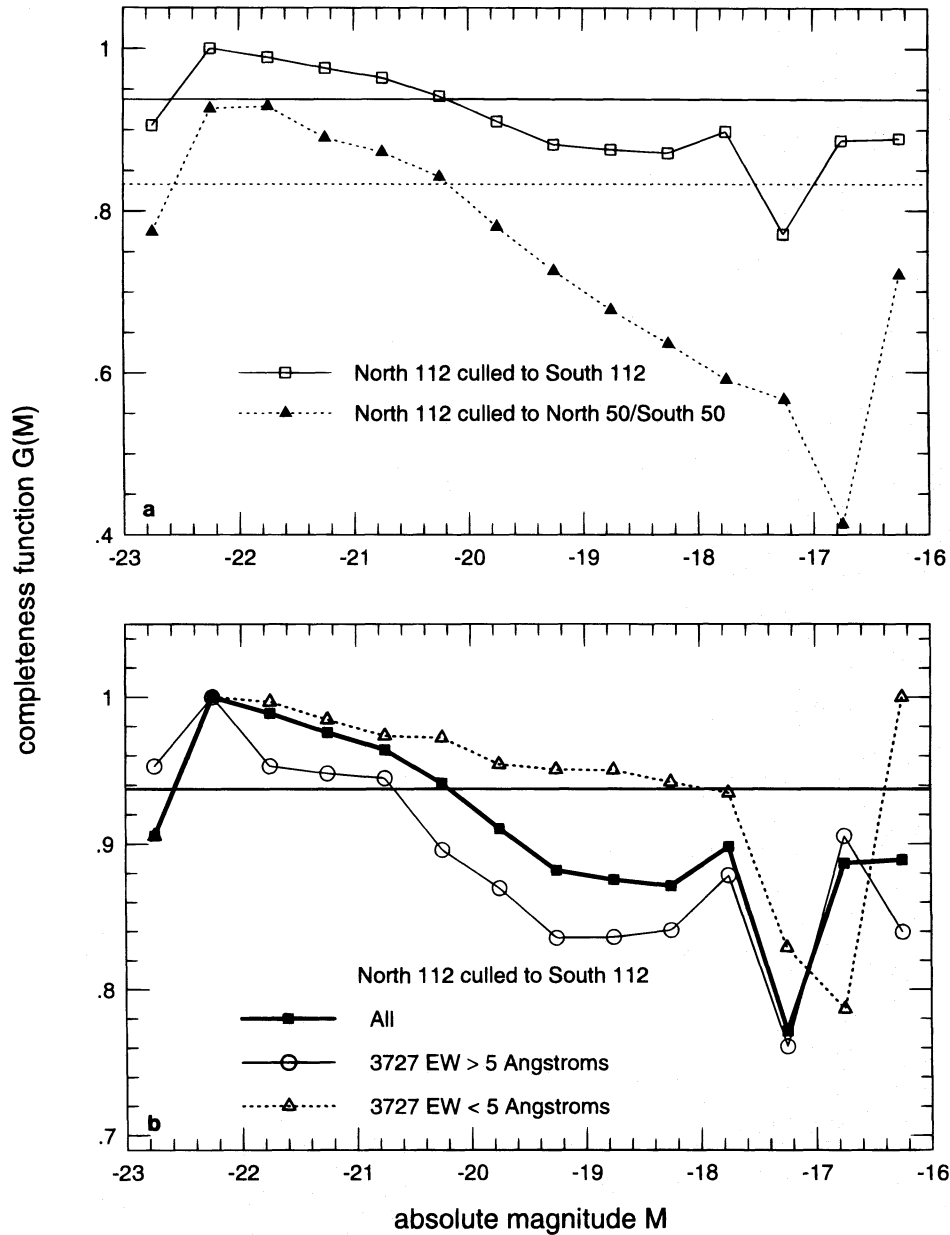$$w(z) = \frac{1}{1 + \bar{f} \bar{\rho} J_3 S(z)}, \tag{27}$$

FIG. 3.—*Top*: Completeness function $G(M)$ vs. absolute magnitude M. $G(M)$ is calculated from the North 112 sample by culling it to match the central surface brightness selection criteria of the North 50/South 50 and South 112 samples. Horizontal lines show the expected values of $G(M)$ if the completeness does not vary with absolute magnitude. *Bottom*: The North 112 sample is again culled to the South 112 sample selection criteria, but now $G(M)$ is separately plotted for all galaxies and for subsets divided by [O II] $\lambda 3727$ equivalent width.

with

$$J_3 = 4\pi \int_0^\infty r^2 \xi(r) dr \tag{28}$$

denoting the second moment of the two-point spatial correlation function $\xi(r)$. We use $J_3 \approx 10{,}000(h^{-1} \text{ Mpc})^3$ as found from a fit to the LCRS real space correlation function (Lin et al. 1996b). Recall ϕ_{obs} is the Schechter function convolved with a Gaussian magnitude error distribution, and the weights W_i account for the sampling and completeness effects (2)–(4) of the previous subsection. Formally, we should also incorporate the completeness effects (3) and (4) into the definition of $S(z)$ above, but since these completeness corrections are generally not too different from unity, it is simpler to use the weights W_i instead. Also, for simplicity, we just use the mean sampling fraction $\bar{f}$ in the denominator of $w(z)$ and ignore the field-to-field variations.

The mean density $\bar{\rho}$ is calculated iteratively using equations (25) and (27). However, we find that for the redshift and absolute magnitude limits we are interested in, 1000 km s^{-1} < cz < 60,000 km s^{-1} and $-23.0 < M < -17.5$, the minimum-variance estimator gives essentially the same $\bar{\rho}$ as when we use inverse selection function weighting,

$$w(z) = 1/S(z) . \tag{29}$$

We will thus adopt this simpler weighting. Nevertheless, we will estimate errors $\delta\bar{\rho}$ in the mean density using the minimum-variance weighting scheme

$$\delta\bar{\rho} \approx \left[\frac{\bar{\rho}/\bar{f}}{\int_{z_1}^{z_2} S(z)w(z)(dV/dz)dz}\right]^{1/2} \sim \bar{\rho}\left(\frac{J_3}{V}\right)^{1/2}. \tag{30}$$

[Here $w(z)$ is that of eq. (27). Note also that the dependence of $\delta\bar{\rho}$ on the actual value of J_3 used is fairly weak.] However, this error estimate accounts just for that part due to galaxy clustering; we add in quadrature the uncertainty in $\bar{\rho}$ arising from varying M^* and α along their joint 1 σ error ellipse. Finally, we can compute the normalization ϕ^* in the Schechter function (8) by

$$\phi^* = \frac{\bar{\rho}}{\int_{M_1}^{M_2} \phi'(M)dM}, \tag{31}$$

where ϕ' is the Schechter function with ϕ^* set to 1. As with $\bar{\rho}$, the errors in ϕ^* will include contributions both from galaxy clustering and from uncertainties in M^* and α.

4. LUMINOSITY FUNCTION AND MEAN DENSITY OF LCRS GALAXIES

Details of the STY fits to the luminosity functions of the N50, S50, N112, S112, and combined NS112 samples are given in Table 2. Two sigma error ellipses, calculated using equation (9) with $\Delta\chi^2 = 6.17$, are plotted in Figure 4. The STY and SWML solutions for the N112, S112, and NS112 samples are shown in Figures 5 and 6. We note first that the N50 and S50 results seem discrepant with the NS112 result. We have verified that we can recover the correct M^* and α parameters, using the methods of §3.2, for the N112 and S112 samples culled to the 50-fiber limits. It is thus unclear why the N50 and S50 samples are still discrepant; the trends of the discrepancies suggest some residual zero-point offset for the S50 sample and some remaining incompleteness in the N50 sample. Since the 50-fiber data constitute just 20% of the whole sample, and since they are subject to larger corrections for central surface brightness selection (Fig. 3 [*top*]), our final quoted results will use just the 112-fiber data, even though the agreement between the N112 and S112 samples is also not quite ideal. The N112 and S112 2σ error ellipses just touch in Figure 4. The M^* values *do* agree well, but the S112 has an α more positive by 0.1 than that of N112. This suggests an incompleteness at the faint end of the luminosity function, but examination of Figure 6 shows instead that the difference arises from an excess of galaxies in the S112 sample at the bright end $M \lesssim -20$. The explanation for this North/South difference is also unclear.

We have done extensive work in eliminating residual field-to-field photometric zero-point offsets in our data; details of the procedures used are given in Shectman et al. (1996). In brief, relative zero-point offsets between our drift scans are removed by comparing data in overlapping regions of the scans and by comparisons to additional CCD calibration frames. Moreover, the effects of variable sky brightness and seeing on our isophotal magnitudes are dealt with by comparing, on a field-by-field
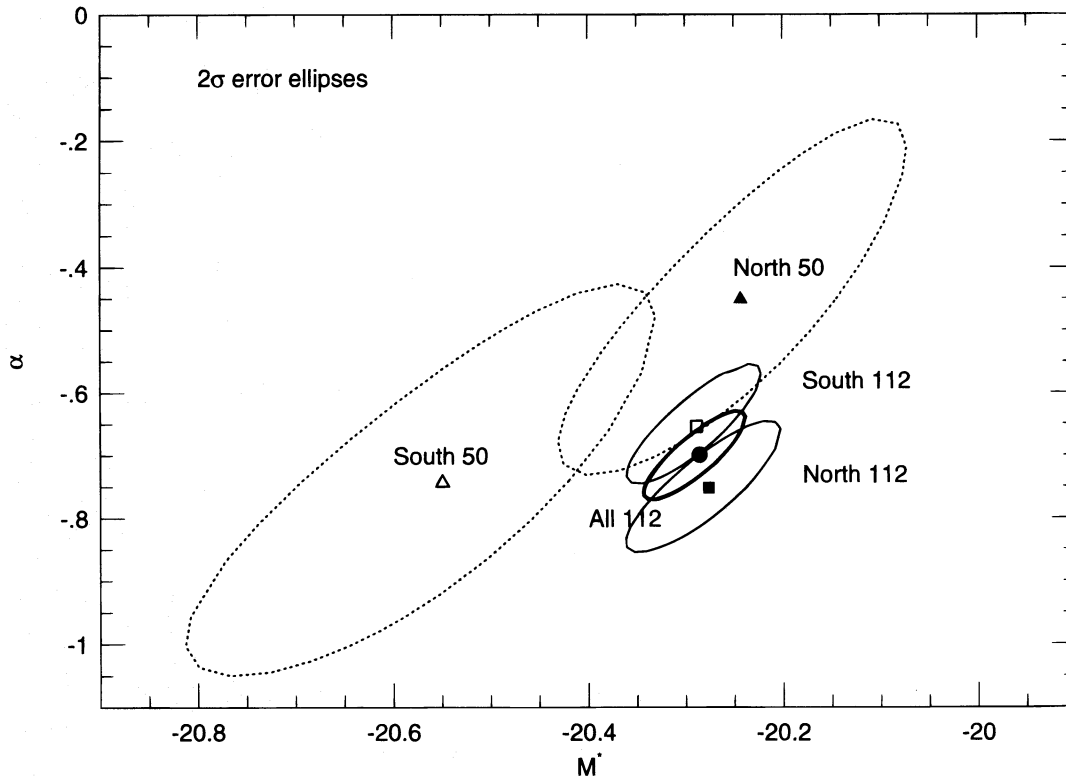

FIG. 4.—2 σ error ellipses in M^* and α for the STY maximum-likelihood fits to the four main subsets of the LCRS data and to the combined North + South 112 sample. Details of the fits are given in Table 2.

TABLE 2
LUMINOSITY FUNCTION PARAMETERS

Sample	N	$M^* - 5 \log h$[a]	α	$\phi^*(h^3 \text{ Mpc}^{-3})$[a]	P_1[b]	P_2[b]
LCRS: [c]						
N50	2690	-20.24 ± 0.07	-0.45 ± 0.11	0.017 ± 0.003	0.20	0.71
S50	2043	-20.55 ± 0.10	-0.74 ± 0.13	0.016 ± 0.003	0.03	0.04
N112	8399	-20.28 ± 0.03	-0.75 ± 0.04	0.018 ± 0.002	0.002	0.004
S112...................	10279	-20.29 ± 0.03	-0.65 ± 0.04	0.020 ± 0.002	0.01	0.06
NS112	18678	-20.29 ± 0.02	-0.70 ± 0.03	0.019 ± 0.001	0.001	0.009
$\lambda 3727 \, W_\lambda \geq 5$ Å......	7312	-20.03 ± 0.03	-0.90 ± 0.04	0.013 ± 0.001	0.24	0.45
$\lambda 3727 \, W_\lambda < 5$ Å......	11366	-20.22 ± 0.02	-0.27 ± 0.04	0.011 ± 0.001	0.002	0.02
Stromlo-APM: [d]						
All	1658	-19.50 ± 0.13	-0.97 ± 0.15	0.0140 ± 0.0017	0.65	...
Early	311	-19.71 ± 0.25	$+0.20 \pm 0.35$	...	0.64	...
Late	999	-19.40 ± 0.16	-0.80 ± 0.20	...	0.87	...
CfA: [e]						
All....................	9063	-18.8 ± 0.3	-1.0 ± 0.2	0.04 ± 0.01	0.25	...
E-S0...................	...	-18.87	-0.92	0.010	...	...
Sa-Sd.................	...	-18.76	-0.81	0.015	...	...
Sm-Im	...	-18.79	-1.87	0.0006 ± 0.0002	0.46	...
SSRS2 [f]	2919	-19.50	-1.20	0.015 ± 0.003	...	...

[a] $H_0 = 100 \, h \text{ km s}^{-1} \text{ Mpc}^{-1}$.

[b] P_1 is probability for likelihood ratio test; P_2 is probability for $dN(M)$ χ^2 test. See § 3.1.

[c] Magnitudes are in our hybrid Kron-Cousins R system and absolute magnitudes are restricted to $-23.0 < M - 5 \log h < -17.5$. ϕ^* is calculated for redshifts $1000 \text{ km s}^{-1} < cz < 60{,}000 \text{ km s}^{-1}$. Errors are formal 1σ uncertainties; but also see discussion in §§ 4 and 6.

[d] Loveday et al. 1992. Magnitudes in b_J system.

[e] Marzke et al. 1994a, b. Magnitudes in Zwicky system.

[f] da Costa et al. 1994. Magnitudes in $B(0)$ system.

basis, the offsets between galaxy isophotal and aperture magnitudes (using a 12″ diameter aperture that should be insensitive to seeing and sky brightness changes). After the correction procedures, the mean photometric zero points from slice to slice showed no offsets greater than ≈ 0.015 mag. It is thus unlikely that zero-point offsets internal to the data can account for the differences seen in Figure 4, particularly the suggestive offset of the S50 sample. Externally, a difference in extinction between
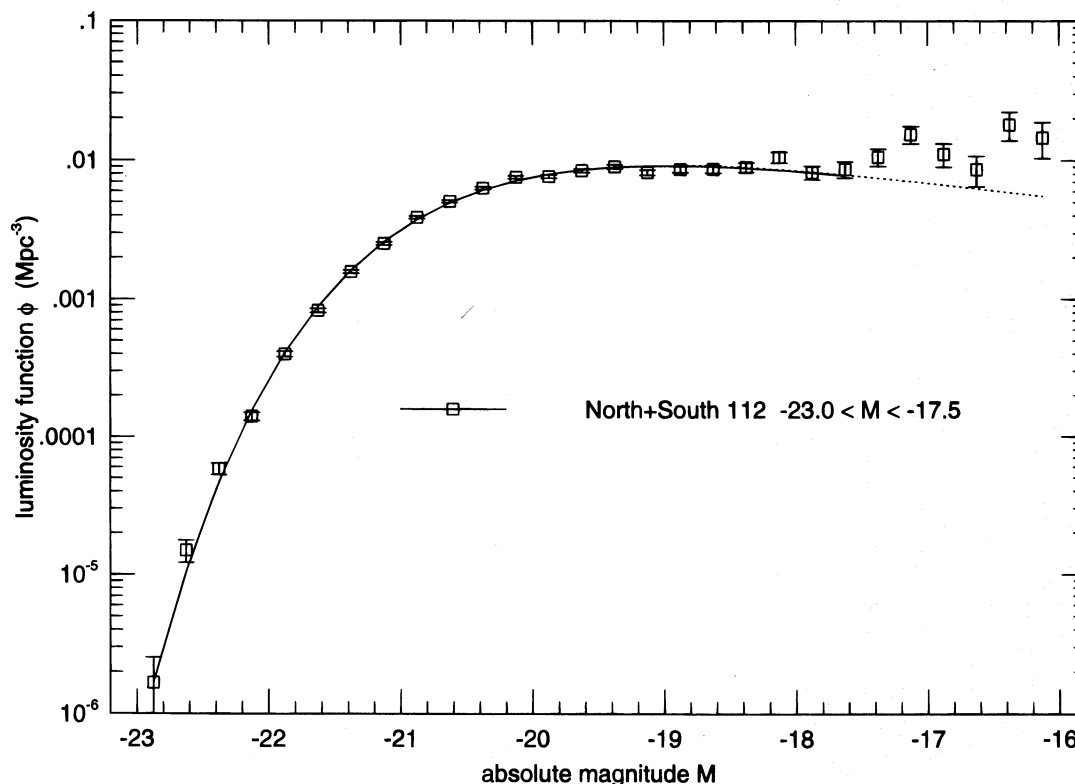

FIG. 5.—Luminosity function for the combined North + South 112 sample. The squares show the SWML solution, plotted with 1 σ errors, and the line shows the STY solution. Details of the STY fit are given in Table 2. The dotted line shows the extrapolation of the fit to $M > -17.5$.
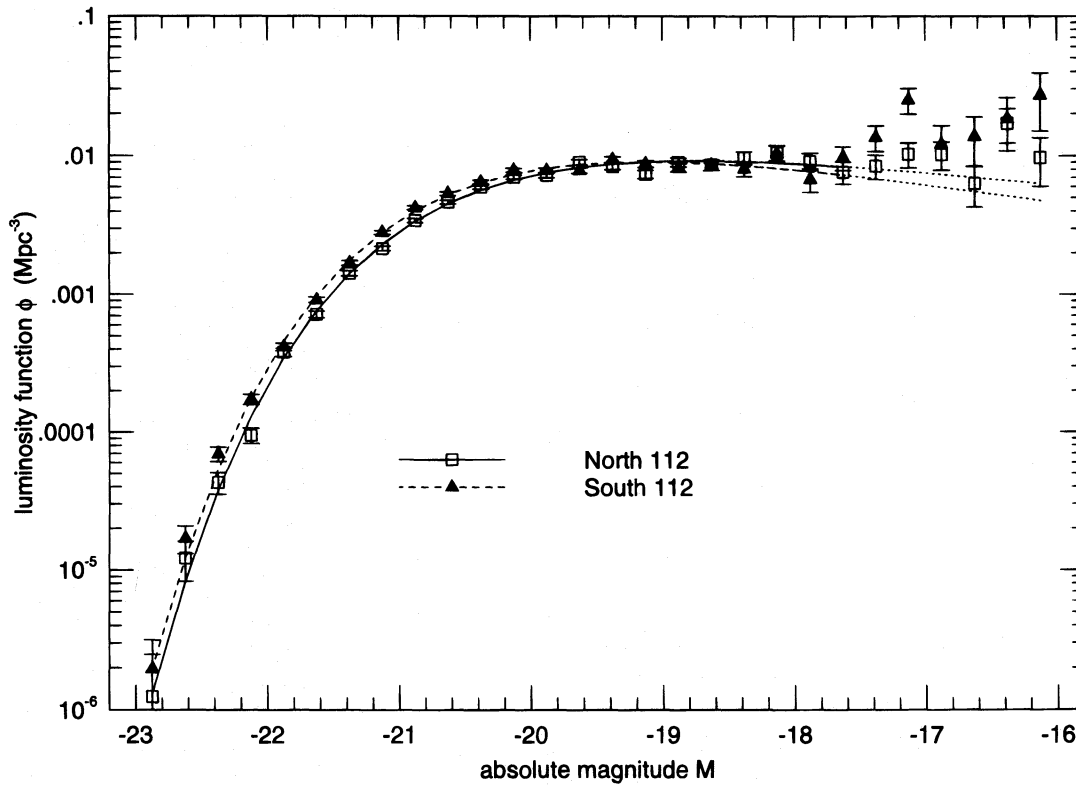
Fig. 6.—Luminosity functions for the North 112 and South 112 samples. The points show the SWML solutions, plotted with 1 σ errors. The lines show the STY solutions, with details of the fits given in Table 2. Dotted lines show the extrapolation of the fits to $M > -17.5$.

the North and South galactic caps comes to mind. We have not made a previous correction for this because 96% of our fields are at high galactic latitudes $|b| \geq 40°$. If we apply an extinction law $\Delta m = -0.07(\csc|b| - 1)$ for $|b| < 50°$ and $\Delta m = 0$ otherwise (Sandage 1973), the changes in both M^* and α are less than 0.02 for all four data sets. An additional extinction of about 0.1 mag in the North relative to the South *could* improve the overlap between the N112 and S112 error ellipses but would not help with the 50-fiber results. Another possibility is that our errors are underestimated. However, we find that the scatter among subsamples of the four main data sets are in fact consistent with the estimated error ellipses for the subsamples. On the other hand, the error estimates do not account for any *intrinsic* variations in the luminosity function parameters with location in the universe. Thus, in particular the N112/S112 discrepancy in α may hint at such cosmic variance, because of the large separation between the samples, but the N50/N112 and S50/S112 differences do not, as these last two pairs of samples are in close proximity. Another point to note is that the image quality for the 112-fiber photometry is appreciably improved over that of the early 50-fiber data photometry, because of the improved CCDs used for the 112-fiber drift scans (Shectman et al. 1995). In any event, whether the sample differences are due to some residual systematic effect(s) or not, we find that the M^* values for the N50, N112, and S112 samples are in good agreement, and we will see below in Table 3 that the galaxy number and luminosity densities for the four main data sets are also consistent within their estimated 2 σ errors. Nevertheless, in light

TABLE 3
Number and Luminosity Densities

Sample	$\bar{\rho}(h^3 \text{ Mpc}^{-3})$[a]	$\rho_L(10^8 L_\odot \, h \text{ Mpc}^{-3})$[a,b]
N50	0.020 ± 0.004	1.2 ± 0.1
S50	0.026 ± 0.006	1.5 ± 0.2
N112	0.028 ± 0.002	1.3 ± 0.1
S112	0.029 ± 0.002	1.5 ± 0.1
NS112	0.029 ± 0.002	1.4 ± 0.1
$\lambda3727 \, W_\lambda \geq 5$ Å......	0.021 ± 0.002	0.74 ± 0.05
$\lambda3727 \, W_\lambda < 5$ Å......	0.011 ± 0.001	0.78 ± 0.04

[a] We take $H_0 = 100 \, h$ km s^{-1} Mpc^{-1}. $\bar{\rho}$ and ρ_L are calculated for absolute magnitudes $-23.0 < M - 5 \log h < -17.5$ and redshifts 1000 km s$^{-1} < cz < 60,000$ km s^{-1}. Errors are formal 1 σ uncertainties.

[b] We assume $R_\odot = 4.52$ (M. Pinsonneault, private communication). Also, be aware that our magnitudes are isophotal and are *not* total; we estimate that our isophotal magnitudes miss roughly 25% of the total light on average.

of the difference in the N112 and S112 α's, we will revise our estimate of the error in α for the NS112 sample upward from the formal value (see below).

The likelihood ratio and χ^2 test (§ 3.1) probabilities P listed in Table 2 show that the Schechter function generally gives only formally marginal fits ($P \geq 0.001$) to the luminosity function of the LCRS samples. Nonetheless, a visual inspection of Figures 5 and 6 shows that the Schechter function is still a useful approximation for the absolute magnitude range $-23.0 \leq M \leq -17.5$. The SWML solutions show excesses relative to the Schechter fits at the faint end $M > -17.5$. We adopt as the LCRS luminosity function the result for the NS112 sample, valid for the range $-23.0 \leq M \leq -17.5$, with 1 σ errors:

$$M^* = -20.29 \pm 0.02 + 5 \log h , \qquad \alpha = -0.70 \pm 0.05 , \qquad \phi^* = 0.019 \pm 0.001 \, h^3 \, \text{Mpc}^{-3} . \qquad (32)$$

Here we conservatively estimate the uncertainty in α to cover the range in α derived from the N112 and S112 samples; the formal error is ± 0.03. Other than this enlargement of the error in α, we note that the errors quoted above and elsewhere in this paper are formal values that should account for random uncertainties in the luminosity function parameters. Systematic uncertainties arising from the following sources should be kept in mind and were discussed previously: completeness corrections (§ 3.2), extinction and photometric calibrations (earlier this section), and cosmology (§ 2).

In our subsequent analyses of the LCRS data (apart from the present paper), we will use the luminosity function values in equations (32) for the N50, N112, and S112 data sets, but for the S50 data set, we use its own luminosity function parameters as given in Table 2. In Figure 7 we plot the selection function $S(cz)$ computed from equation (26) using the M^* and α values for each of our four data sets and for the combined NS112 sample, while restricting the absolute magnitudes to $-23.0 \leq M \leq -17.5$. Note the typical decline at high cz caused by the survey's faint apparent magnitude limits. However, there is also a decline at small cz, a result of the survey's additional bright apparent magnitude limits.

The mean densities computed for the LCRS samples are given in Table 3. We plot in Figure 8a the galaxy density ρ as a function of redshift cz, for galaxies in the NS112 sample within absolute magnitude limits $-23.0 \leq M \leq -17.5$. We also plot the cumulative density for galaxies lying within redshift cz, showing that the density appears to have converged within the LCRS survey volume. We stop at $cz = 60,000$ km s^{-1}, where the selection function $S(cz)$ has dropped to approximately 0.01 (Fig. 7). We find a mean density $\bar{\rho} = 0.029 \pm 0.002$ galaxies h^3 Mpc^{-3}. Galaxy clustering contributes a 4% fractional uncertainty to $\bar{\rho}$, and uncertainties in the luminosity function parameters contribute another fractional uncertainty of 4%. Note from Table 3 that despite the difference in α values, the mean densities of the N112 and S112 samples do in fact agree well. To compare the N112 and S112 radial density distributions in more detail, we also plot, as a function of cz, the ratio of the N112 to S112 galaxy number densities (Fig. 8c) and galaxy number histograms (Fig. 8d; account has been made of the differences in volume and completeness). Note that the ratios differ somewhat in the two figures, since the density ratios include the effect of the differing N112/S112 luminosity functions, but the histogram ratios do not. We find from either plot
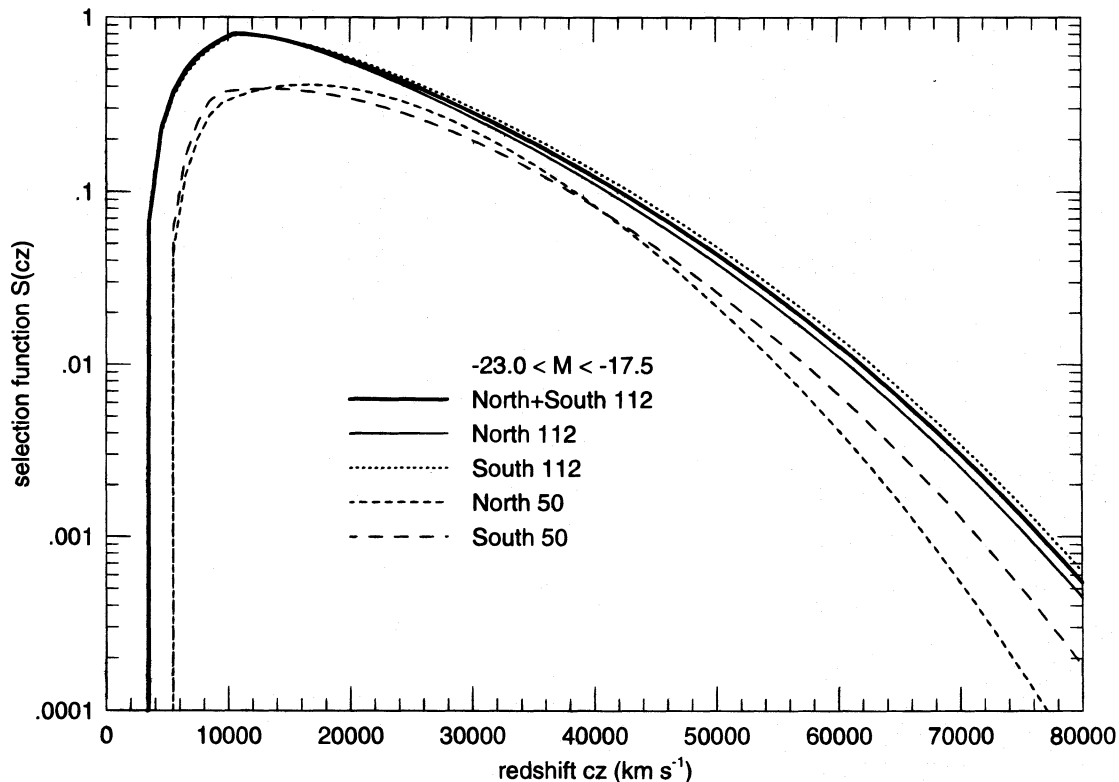

Fig. 7.—Selection function $S(cz)$, computed using the luminosity function parameters and nominal apparent magnitude limits of each of the North 50, South 50, North 112, South 112, and combined North + South 112 samples. Absolute magnitude limits $-23.0 \leq M \leq -17.5$ have also been applied.
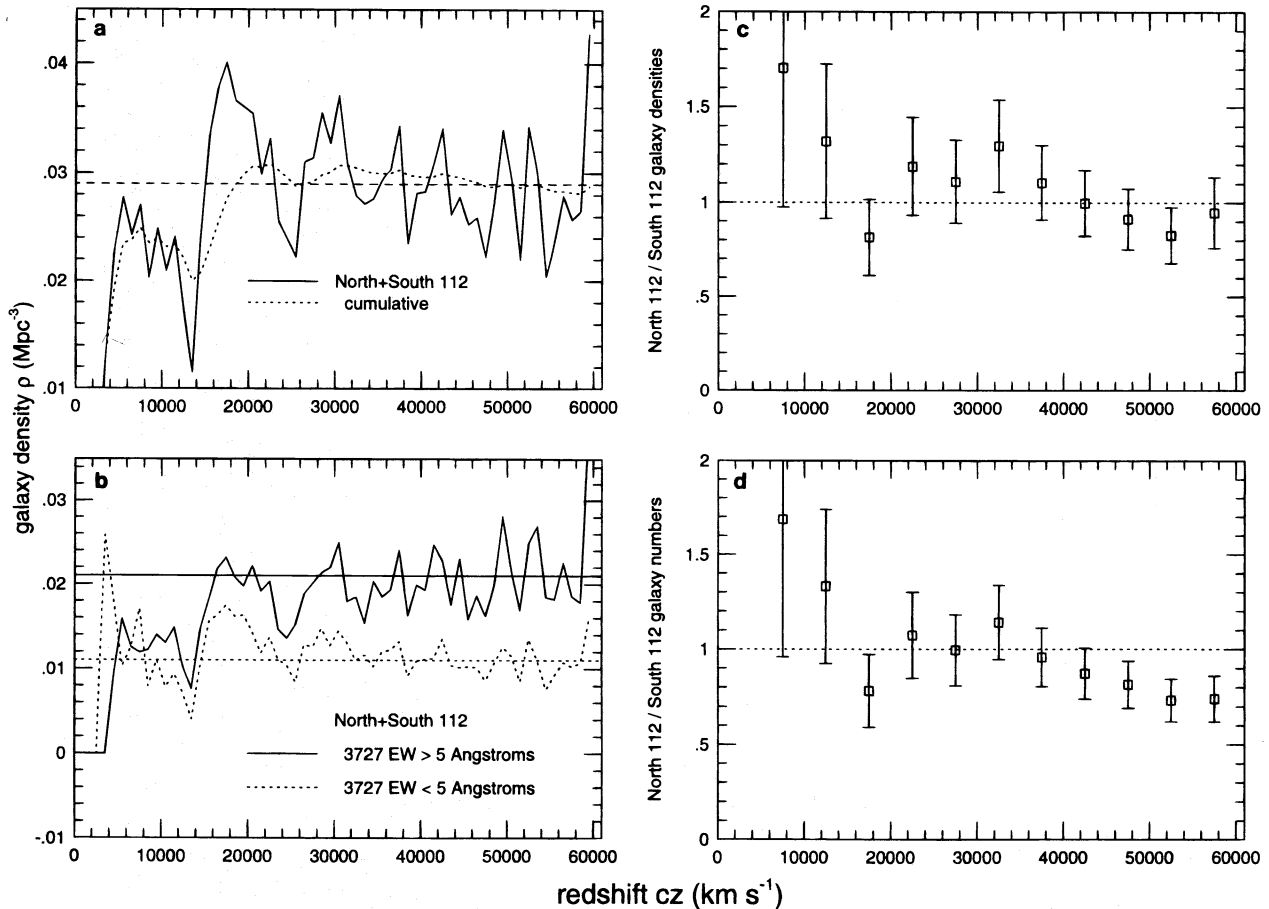
FIG. 8.—Galaxy density ρ as a function of redshift cz for (a) the whole North + South 112 sample and (b) the North + South 112 sample divided by $\lambda 3727$ emission. The horizontal lines show the respective mean densities; see Table 3. The ratio of the North 112 over the South 112 (c) galaxy number densities and (d) normalized galaxy number histograms are also shown. The errors bars in (c–d) are described in the text. In all cases, the absolute magnitude range is $-23.0 \leq M \leq -17.5$.

that for radial shells of thickness 5000 km s^{-1}, fluctuations in galaxy numbers and densities of about 20% between N112 and S112 are not uncommon. In particular, the decline seen in the N112 sample for $cz \gtrsim 40,000$ km s^{-1} is consistent with the deficit of $M \lesssim M^*$ galaxies observed in the N112 versus S112 luminosity functions (Fig. 6). On the other hand, we also plot, as error bars on the ratios, the expected fluctuations arising from the combination of galaxy clustering, shot noise, and uncertainties in M^* and α (the last only for the density ratios). In computing the galaxy clustering component of the fluctuations we have accounted for the geometry of the shells and used a fit to the LCRS power spectrum (Lin et al. 1996a; this procedure is preferred over the approximate error estimate of eq. [30], which tends to give an overestimate given the geometry of the shells). We see that the observed density fluctuations between N112 and S112 appear to be consistent with the expectations, despite the 2 σ discrepancies between the N112/S112 M^*-α error ellipses. The N112/S112 luminosity functions thus do not differ significantly in normalization (as described by the galaxy number densities) but do differ in shape (specifically in α).

We also tabulate in Table 3 the galaxy luminosity density ρ_L, given by

$$\rho_L = \int_{-23.0}^{-17.5} 10^{-0.4M^*} \phi(M) dM .\qquad(33)$$

(Letting the integration limits go to infinity only increases ρ_L by 3%.) The NS112 value of $(1.4 \pm 0.1) \times 10^8 L_\odot h$ Mpc^{-3}, when increased by 25% as a rough isophotal-to-total light correction, implies a critical mass-to-light ratio $(M/L) \approx 1.6 \times 10^3 (M/L)_\odot$ to close the universe, in agreement with previous determinations (see, e.g., Kirshner et al. 1983; EEP; Marzke et al. 1994b). Alternatively, we obtain a cosmological density parameter $\Omega \approx 0.2[(M/L)/300 h (M/L)_\odot]$, if we set $M/L = 300 h (M/L)_\odot$, a typical virial mass-to-light ratio estimated from clusters and groups [e.g., a recent determination from the CNOC cluster sample gives $M/L = 295 h (M/L)_\odot$ in Gunn r; Carlberg et al. 1996].

In addition, we have also derived ϕ^* for the NS112 sample by normalizing to our galaxy number count distribution $dn(m)$. We use

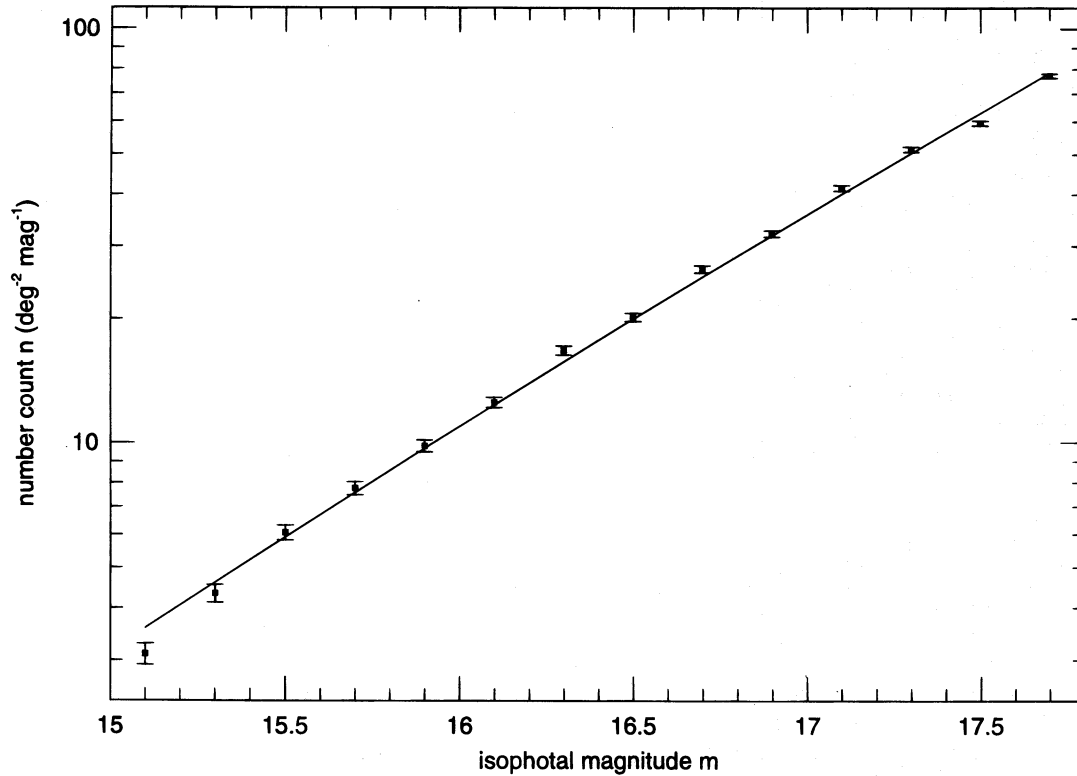$$\int_m^{m+\Delta m} dn(m) = \int_0^\infty dz(dV/dz) \int_M^{M+\Delta M} \phi_{\text{obs}}(M') dM' ,\qquad(34)$$

FIG. 9.—Number count n as a function of isophotal magnitude m for the North + South 112 photometric catalog. Poisson errors are shown. A 3% correction has been applied to account for stellar contamination. The solid line shows the prediction derived from the NS112 luminosity function, with normalization fixed by the number counts.

and do a χ^2 fit to find ϕ^*, assuming Poisson errors on the counts, and fixing M^* and α at their maximum-likelihood values. For the counts we consider *all* objects in our CCD photometric catalog with isophotal magnitudes $15.0 \leq m \leq 17.8$, except that we make a 3% correction for stellar contamination, as inferred from the fraction of stars in our spectroscopic sample. We find $\phi^* = 0.021\ h^3$ Mpc^{-3}, but to compare properly against our redshift survey value, we need to make a 4% reduction to
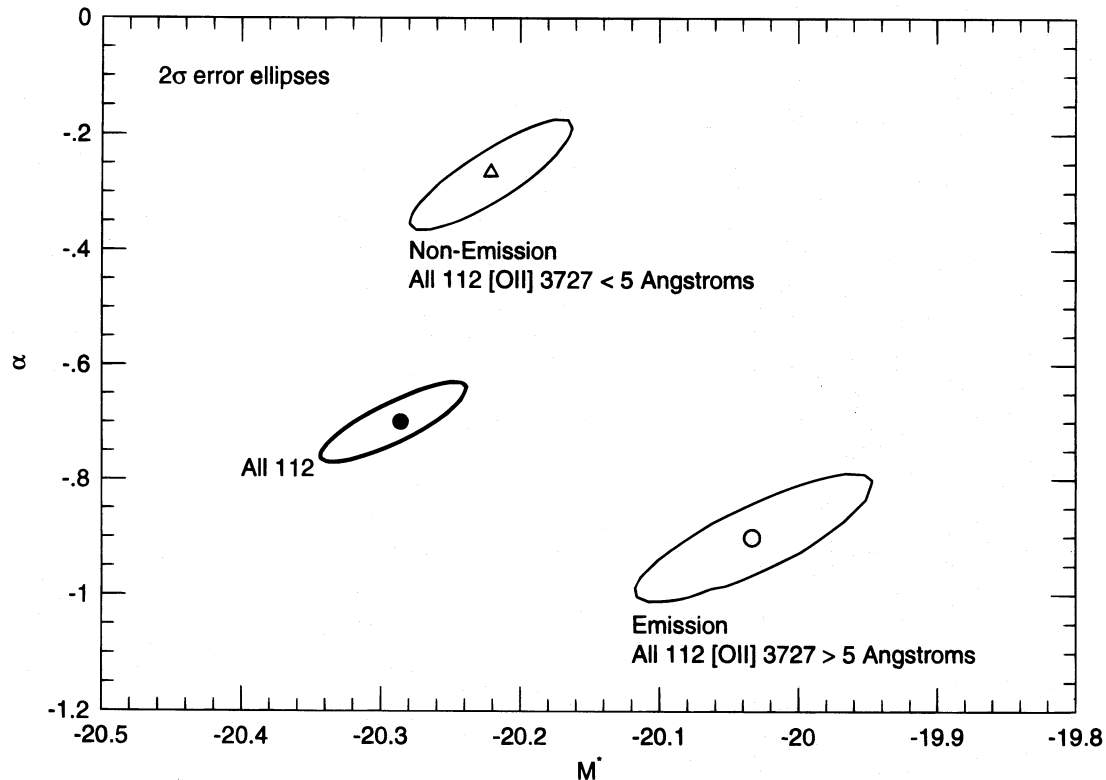

FIG. 10.—2 σ error ellipses in M^* and α for the STY maximum-likelihood fits to the combined North + South 112 sample, whole and divided into two subsets by [O II] $\lambda 3727$ equivalent width. Details of the fits are given in Table 2.
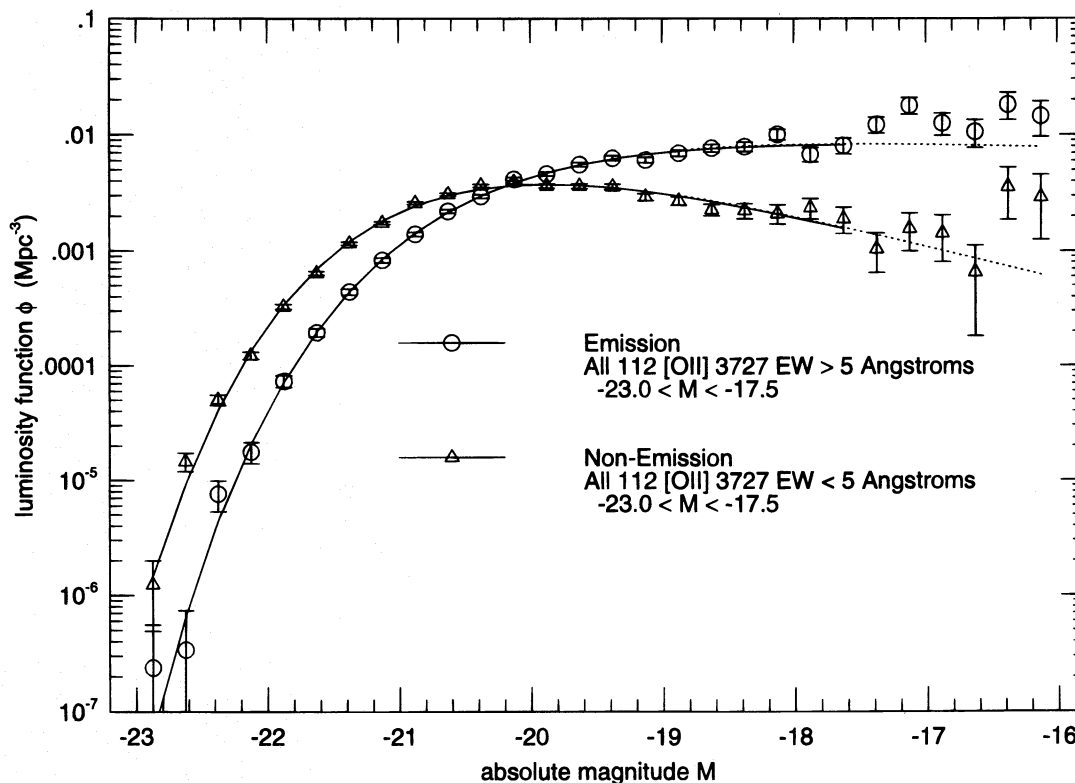
FIG. 11.—Luminosity functions for the combined North + South 112 sample, divided by [O II] $\lambda 3727$ equivalent width. The points show the SWML solutions, plotted with 1 σ errors. The lines show the STY solutions, with details of the fits given in Table 2. Dotted lines show the extrapolation of the fits to $M > -17.5$.

account for the low surface brightness galaxies excluded from the redshift survey. We get $\phi^* = 0.020\ h^3$ Mpc^{-3}, in good agreement with the value $\phi^* = 0.019 \pm 0.001\ h^3$ Mpc^{-3} derived from the redshift survey. We show in Figure 9 the $dn(m)$ distribution for the NS112 sample and the prediction based on $\phi^* = 0.021\ h^3$ Mpc^{-3}, $M^* = -20.29$, and $\alpha = -0.70$.

We have also separated the NS112 sample into two groups by [O II] $\lambda 3727$ emission, defining emission galaxies to be those with $\lambda 3727$ equivalent widths $W_\lambda \geq 5$ Å. The emission galaxies constitute 40% of the total sample. The fit details are given in Table 2, the error ellipses are plotted in Figure 10, and the SWML and STY solutions are shown in Figure 11. Note that for the S112 data, we have used separate surface brightness completeness functions $G(M)$, shown in Figure 3b, for the emission and nonemission galaxies. We see that emission and nonemission galaxies have very different luminosity functions, with emission galaxies dominating the faint end and nonemission galaxies prevailing in the bright end. In particular, emission galaxies constitute about 15% of the total at $M = -22$, rising to about 80% at $M = -17$. The two populations show about equal number densities near the full sample M^*. The emission galaxies show a much steeper faint end slope α (-0.9 vs. -0.3) and a slightly fainter M^* (-20.0 vs. -20.2) relative to the nonemission galaxies. Also, note from Figure 11 that the excesses at $M > -17.5$ relative to the Schechter fits are less pronounced than they were for the full sample, though for consistency we use the same fit range $-23.0 \leq M \leq -17.5$. Moreover, the probabilities in Table 2 indicate that a Schechter function is a good description of the emission galaxy luminosity function, though again visual inspection of Figure 11 indicates that the Schechter function provides reasonable (though not always *formally* good) approximations to the luminosity functions of both subsamples. In Figure 8b, we plot the space density of emission and nonemission galaxies. Finally, we note that instead of our formal 1 σ errors for α listed in Table 2, we quote instead an error of ± 0.1 for both the emission and nonemission galaxies. We do this because of our earlier N112/S112 difference in α and because of another effect to be discussed at the end of § 6.

5. COMPARISONS TO OTHER SURVEYS

We next compare our luminosity function to that from three other large, local, and optically selected redshift surveys. The luminosity functions from the Stromlo-APM (Loveday et al. 1992), Center for Astrophysics (CfA; Marzke et al. 1994b), and second Southern Sky (SSRS2; da Costa et al. 1994) redshift surveys are detailed in Table 2 and are plotted against that of the LCRS NS112 sample in Figure 12. Because these other surveys were selected in the blue, while the LCRS was selected in the red, for the comparison we need to shift the zero points of the various magnitude systems. (Shifting the zero points also roughly accounts for other differences in the magnitude systems; e.g., the fact that LCRS magnitudes are explicitly isophotal, whereas APM magnitudes have an isophotal-to-total magnitude correction applied. However, applying simple constant offsets does neglect more complicated effects, which are due, for example, to galaxy colors and morphologies. Be aware that the specific differences we find below in the luminosity functions will necessarily be sensitive to the exact shifts in absolute magnitudes we apply.) For Stromlo APM we have offset its M_{b_j} magnitude scale by 1.1 mag to match approximately the mean rest-frame color $\langle b_j - R \rangle_0 = 1.1$ of LCRS galaxies (Tucker 1994; Tucker et al. 1995). We shift the SSRS2 $M_{B(0)}$ magnitude
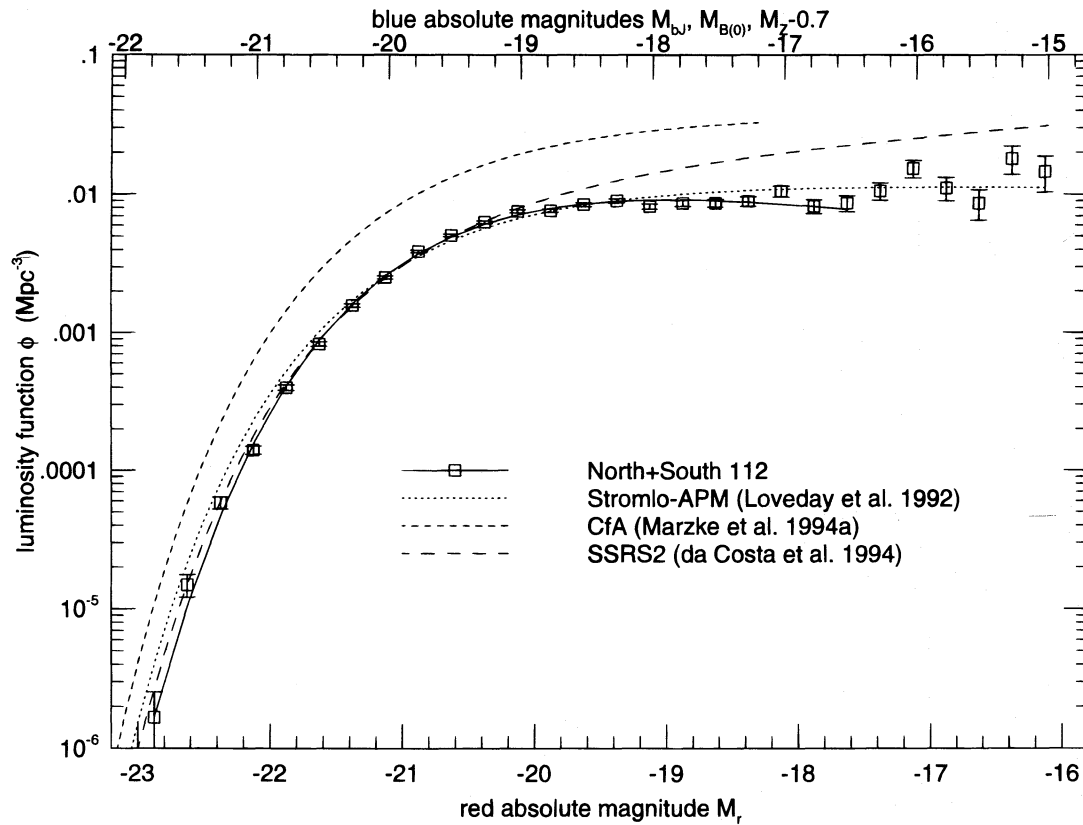
Fig. 12.—Luminosity function for the combined North + South 112 LCRS sample, compared to those of the blue-selected Stromlo-APM, CfA, and SSRS2 surveys. Note that the blue M_{b_J} and $M_{B(0)}$ (top) and red M_r (bottom) absolute magnitude scales are offset in order to match the average color $\langle b_J - R \rangle_0 = 1.1$ of LCRS galaxies. The blue Zwicky M_Z magnitude scale has been shifted to match the CfA and Stromlo-APM M^* values. The CfA results show an excess relative to the plotted fit at $M_Z \gtrsim -16$; see Marzke et al. (1994b).

scale by the same amount, since the SSRS2 and b_J zero points agree within 0.2 mag (da Costa et al. 1994). However, we shift the Zwicky M_Z magnitude scale for the CfA survey by another 0.7 mag to match the CfA and Stromlo-APM M^* values. Note first from the figure that the Stromlo-APM and LCRS results show consistent normalizations and are fairly similar in overall shape, despite differences in their respective Schechter parameters, particularly in the faint-end slope α. There are instead differences, for $M_r \lesssim -21.5$ and $M_r \gtrsim -19$, which are responsible for the shallow faint-end slope $\alpha = -0.7$ found in the LCRS, compared to the more typical flat value $\alpha \approx -1$ seen in the Stromlo-APM and other previous surveys. We emphasize that even though the LCRS is slightly biased against intrinsically faint galaxies (because of the survey selection criteria and the correlation between luminosity and central surface brightness), the *gross* features of our luminosity function are quite similar to an $\alpha = -1$ Schechter function. However, such a Schechter function does not provide as good a fit in *detail* to the LCRS data. As another aid in the comparison, note that for $-1 \leq \alpha \leq -0.7$, we roughly have $(\Delta \rho_L / \rho_L) \approx (\Delta \phi^*/\phi^*) - 0.9 \Delta M^* + \frac{1}{3}(\Delta \alpha / \alpha)$ (good to about 0.1 in $\Delta \rho_L/\rho_L$). Thus, the LCRS and Stromlo-APM surveys have about the same luminosity density ρ_L despite their different Schechter parameters (Table 2): the 30% difference in ϕ^* is more than compensated for by the 30% difference in M^* (after noting the 1.1 mag zero-point shift) and one-third of the 30% difference in α.

We note next from Figure 12 that the CfA and SSRS2 luminosity functions show some conspicuous differences compared to the LCRS and Stromlo-APM results. The CfA luminosity function clearly shows a higher normalization, though its shape is similar as it has $\alpha = -1$. On the other hand, the SSRS2 luminosity function is quite similar to those of the LCRS and Stromlo-APM surveys for $M_{b_J} \lesssim -19$, but for fainter magnitudes its $\alpha = -1.2$ makes the SSRS2 result overshoot the LCRS and Stromlo-APM luminosity functions. Though not shown in the figure, the CfA luminosity function also has a similar excess at faint magnitudes $M_Z \gtrsim -16$ relative to an extrapolation of the $\alpha = -1$ fit (see Fig. 9 of Marzke et al. 1994b). It is unclear why such a steep faint end (see below) is not observed in the LCRS or Stromlo-APM surveys. However, the high normalization of the CfA survey may be explained as the result of local density inhomogeneities (e.g., large coherent structures like the "Great Wall"; Geller & Huchra 1989) present in the CfA survey volume. Both the CfA and SSRS2 surveys probe a smaller and more local volume of space compared to either the LCRS or Stromlo-APM surveys; the mean survey depths are about 7500 km s^{-1} for both CfA and SSRS2, 15,000 km s^{-1} for Stromlo-APM, and 30,000 km s^{-1} for the LCRS. In fact Marzke et al. (1994a) and da Costa et al. (1994) both point out that their respective surveys are not yet large enough to be "fair" samples of the universe. Both the LCRS and Stromlo-APM surveys should come closer to representing fair samples, and it is remarkable that their respective luminosity functions are quite similar in both normalization and shape.

We do not have morphological classifications for our survey galaxies. Nonetheless, though there is not a one-to-one correspondence between $\lambda 3727$ emission and morphological type, we do expect our emission galaxies to tend to be late-type spirals and our nonemission galaxies to be early-type ellipticals and S0's. We also tabulate in Table 2 the luminosity function

for galaxies of different morphological types computed for the Stromlo-APM and CfA (Marzke et al. 1994a) surveys. The sharp distinction in α between the early- and late-type luminosity functions in the Stromlo-APM survey ($\alpha = +0.2$ and -0.8, respectively) qualitatively agrees with the emission versus nonemission differences seen in the LCRS. However, Zucca et al. (1994) and Marzke et al. (1994b) suggest that incomplete classification of early-type galaxies may be responsible for the difference seen in the Stromlo-APM survey. In fact, there is no significant difference in the luminosity functions of E-S0 and spiral (Sa-Sd) luminosity functions in the CfA survey ($\alpha = -0.8$ to -0.9). However, Marzke et al. (1994b) do find that their faint end is dominated by Magellanic spiral and irregular galaxies, with a very steep $\alpha = -1.87$. Moreover, da Costa et al. (1994) attribute their steep $\alpha = -1.2$ to the dominance of blue galaxies at the faint end. These CfA and SSRS2 results are in qualitative agreement with the LCRS findings, as we expect such late-type blue galaxies to be gas rich and to exhibit strong emission lines.

6. RELATION TO GALAXY COUNTS AND GALAXY EVOLUTION

The problem of the excess faint blue galaxy counts over the expectations of the simplest no-evolution models has continued to be an area of intense research (see reviews by Koo & Kron 1992; Koo 1995). The absence in deep pencil beam redshift surveys (Broadhurst, Ellis, & Shanks 1988; Colless et al. 1990, 1993; Glazebrook et al. 1995a) of high-redshift $z \gtrsim 1$ galaxies, which are predicted by simple luminosity evolution models for the excess counts, has led to proposals of more exotic explanations. For example, the excess blue galaxies may be star-bursting dwarfs that have since faded by the present day (e.g., Broadhurst et al. 1988; Cowie, Songaila, & Hu 1991; Babul & Rees 1992), or, alternatively, extensive galaxy merging may have occurred to remove the excess galaxy population by $z = 0$ (Broadhurst, Ellis, & Glazebrook 1992; Rocca-Volmerange & Guiderdoni 1990).

In contrast, other workers (Gronwall & Koo 1995; Koo, Gronwall, & Bruzual 1993; Metcalfe et al. 1991, 1995b) have argued that the data may still be reasonably fitted by mild evolution models, given the uncertainties in the faint-end slope and in the normalization of the local luminosity function; note in particular the steep α of the Sm-Im sample of Marzke et al. (1994b), and the difference in normalization between the Stromlo-APM and CfA surveys. In fact, even before the CfA results, the counts in the APM galaxy catalog (Maddox et al. 1990a) at *bright* magnitudes $b_J = 20.5$ showed a factor of 2 excess relative to no-evolution predictions based on the counts at $b_J \approx 17$ (Maddox et al. 1990b). Either significant evolution occurred at *low* redshifts $z \approx 0.1$ (Maddox et al. 1990b) or there are large-scale structures (voids) and/or magnitude scale errors (Metcalfe, Fong, & Shanks 1995a) in the APM survey that are biasing the $b_J \approx 17$ counts systematically low. Choosing to normalize to the galaxy counts at $b_J \approx 20$ corresponds to using $\phi^* = 0.03\ h^3$ Mpc^{-3}, twice the Stromlo-APM value, and using this high normalization reduces the amount of evolution needed to reconcile with the faint count data.

There is now evidence from deep redshift surveys for evolution in the luminosity function since redshifts $z \approx 0.5$ (Eales 1993; Lonsdale & Chokshi 1993), but one which depends on galaxy type. Blue, star-forming galaxies appear to exhibit an increased density and/or steepening faint-end slope with increasing redshift, whereas the red galaxy population shows no evolution with z (Lilly et al. 1995; Colless 1995). There is also evidence of an increase in star formation rate with redshift and the association of merging activity with increased star formation (Colless 1995; Colless et al. 1994). In particular, the number of star-forming galaxies, defined as those with [O II] $\lambda3727\ W_\lambda > 20$ Å, appears to be 5–10 times greater at $z \gtrsim 0.5$ than at $z = 0$, for absolute magnitudes below and including M^* (Colless 1995). In addition, recent galaxy number counts from the *Hubble Space Telescope* (*HST*) Medium Deep Survey (Glazebrook et al. 1995b; Driver, Windhorst, & Griffiths 1995a; Driver et al. 1995b) indicate that at $B \approx 24$, the counts are dominated by galaxies with irregular and peculiar morphologies, which show increased numbers relative to their proportions in local surveys. However, the elliptical and spiral counts are as expected with no evolution needed, if one adopts the Stromlo-APM luminosity function, but with the *high* normalization $\phi^* = 0.03\ h^3$ Mpc^{-3}.

It is beyond the scope of this paper to undertake detailed modeling of the evolution of galaxies, but results from the local LCRS sample bear on two points that may be connected to understanding the faint blue galaxies. One is the normalization of the local luminosity function, and the other is the rate of evolution for galaxies with active star formation. First, we note that our luminosity function normalization is consistent with the low value from the Stromlo-APM survey, not with the high value implied by the $b_J \approx 20$ APM galaxy counts. Thus, results arguing for no or mild evolution, e.g., the luminosity function models of Gronwall & Koo (1995) or the *HST* elliptical and spiral counts, will need to be modified if our low normalization is not an underestimate. Because of our large survey depth, up to $z = 0.2$, large-scale structures should not bias our results low (cf. Fig. 8). The normalizations for the two completely independent samples N112 and S112, which probe opposite directions in the sky, agree well with each other. Also, the remaining 4% of low central surface brightness galaxies that are not part of the redshift survey will not lead to such a large underestimate. We saw before that our ϕ^* normalization is consistent with our total number counts, *including* the low surface brightness galaxies. Any potential factor of 2 underestimate will have to come from galaxies completely missing from our original CCD photometric catalog, because they lie below our effective surface brightness limit. Such a bias against very low surface brightness galaxies, as has been argued for by, e.g., McGaugh (1994) and Ferguson & McGaugh (1995), would be a potential problem for all bright galaxy surveys, not just the LCRS. We have derived a firm value for the density normalization of galaxies with central surface brightnesses *above* our explicit cut line(s), examples of which are shown in Figure 1. A final observation here is that our galaxy counts, for our hybrid Kron-Cousins $R = 15$–17.8, correspond roughly to $b_J = 16$–19. However, whereas the APM counts over this range seem too steep at face value to be consistent with no evolution, even at such bright magnitudes (Maddox et al. 1990b), the Las Campanas counts shown in Figure 9 at comparable magnitudes suggest no such evidence for evolution at low redshifts $z \approx 0.1$.

Second, we address the possibility of an increase in the number of star-forming galaxies at redshifts $z < 0.2$ explored by the LCRS, as has been observed by redshifts $z \approx 0.3$ in deeper surveys (Colless 1995), by checking whether the average equivalent width of [O II] $\lambda3727$ varies with redshift. To factor out the dependence of [O II] $\lambda3727\ W_\lambda$ on galaxy luminosity, we plot in
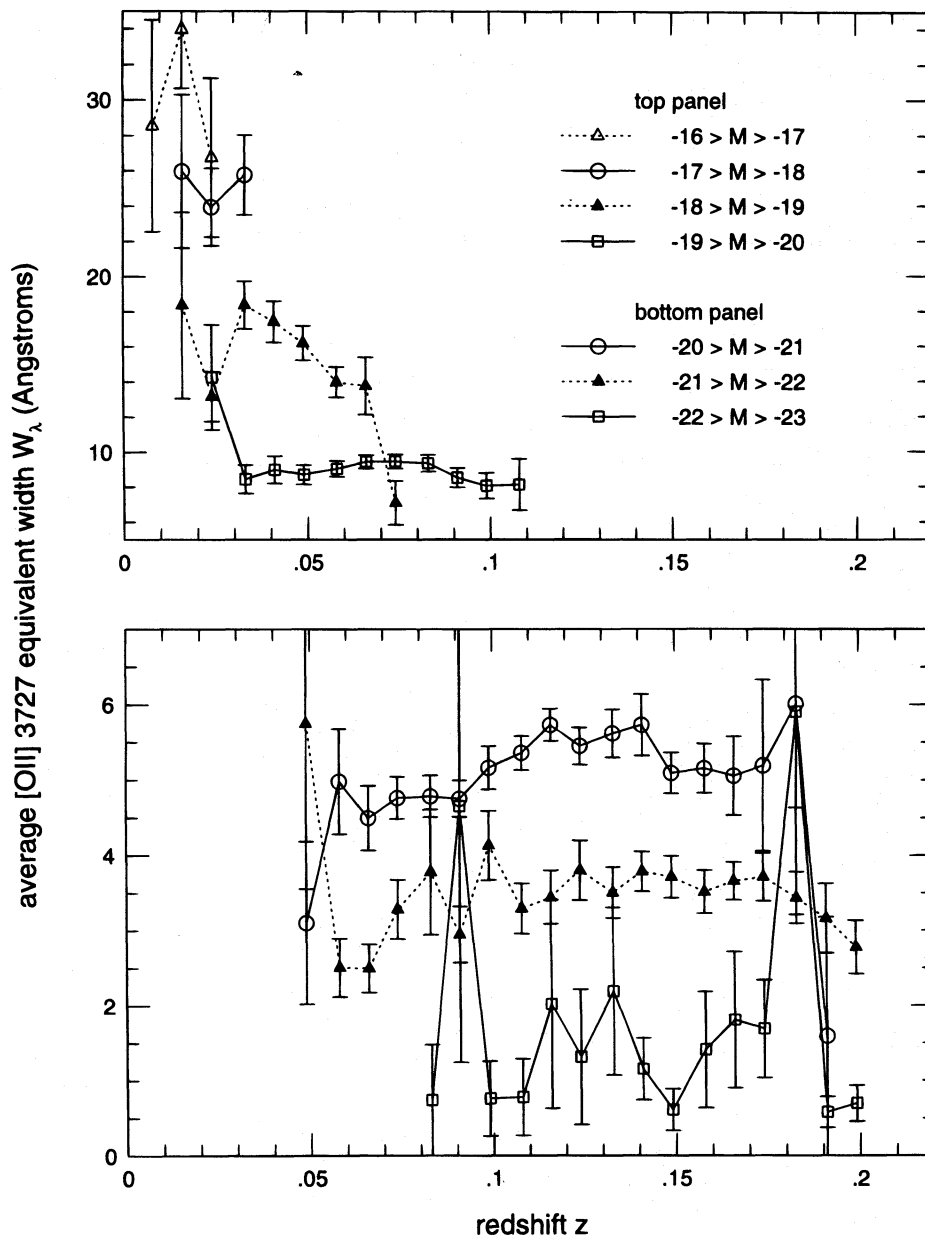
FIG. 13.—Average [O II] λ3727 equivalent width as a function of redshift, computed for galaxies in the LCRS North + South 112 sample. The galaxies have been divided into seven bins in absolute magnitude, each 1 mag wide, ranging from $M = -16$ to -23. The errors shown are standard deviations of the mean.

Figure 13 the average W_λ as a function of z for seven separate absolute magnitude bins, each 1 mag wide, from $M = -16$ to -23. We use only our NS112 data. Our results indicate that the average equivalent widths generally do not change with redshift, although for galaxies fainter than $M = -19$, the redshift range is not large. A similar conclusion may also be drawn by plotting the fraction of galaxies with, say, $W_\lambda > 5$ Å or 20 Å. In light of the error bars, the most significant trend seen is that for the $-20 > M > -21$ bin, specifically a rise of about 1 Å in the average W_λ at $z \approx 0.1$. This may be due to large-scale structure, as the same trend is less apparent in the N112 sample than in the S112 sample. Alternatively, it may be an aperture effect, in that our 3″5 diameter fibers cover 5 h^{-1} kpc on a galaxy at $z = 0.1$, but only half as much at $z = 0.05$, so that there would be a bias toward lower equivalent widths at lower redshifts if less emission arose from the centers of galaxies compared to that from the outer regions. An argument against the latter explanation is that we do not see any consistent systematic trend of this kind in the other absolute magnitude bins. In any event, the evidence for changes in W_λ is not dramatic in any of the luminosity bins. Since λ3727 equivalent width is a surrogate for the star formation rate (Kennicutt 1992), we conclude that there is no evidence for significant evolution in the star-forming properties of LCRS galaxies over the redshift range we sample. We emphasize that this conclusion is only valid over the *respective* redshift ranges observable for galaxies of different luminosities, and that galaxies fainter than $M^* + 1 \approx -19$ are not seen above $z = 0.1$. For galaxies brighter than M^*, though, our no-evolution result does extend up to $z = 0.2$. However, note that our null results say nothing about the above-mentioned evidence of increasing numbers of star-forming galaxies at *higher* redshifts than that constrained by the LCRS, specifically an increase for sub-M^* galaxies by $z \approx 0.3$ and for M^* galaxies by $z \approx 0.5$ (Colless 1995).

A final note is that the small increase in W_λ seen for M^* galaxies does have some impact on the α value derived earlier for our emission and nonemission galaxy samples. In fact, in our earlier derivation we actually applied redshift-dependent weights, analogous to the completeness corrections discussed in § 3.2, to account for any changes in the emission (or nonemission) galaxy fraction as a function of z. The weights are calculated separately for galaxies of different absolute luminosities. If we had not applied such corrections, the maximum-likelihood solution for the emission galaxy α would steepen by -0.1, while the nonemission α would flatten by $+0.1$. Leaving out the additional corrections leads primarily to a systematic increase in the emission galaxy density with redshift (because of the steeper α), so that the sum of the cumulative emission and nonemission galaxy densities overshoots that for all galaxies by about 25% at the $cz = 60,000$ km s^{-1} limit. In light of the lack of evolution seen in the Figure 13 results, which do *not* depend on the luminosity function, we feel justified in applying the z-dependent corrections, resulting in more reasonable agreement between the total galaxy density and the sum of the emission and nonemission galaxy densities given in Table 3. We increase our estimated errors in the emission and nonemission α's to ± 0.1 in light of the above effects, as we alluded to before at the end of § 4.

7. CONCLUSIONS

We have used inhomogeneity-independent maximum-likelihood methods to calculate the luminosity function of LCRS galaxies in the (hybrid) Kron-Cousins R absolute magnitude range $-23.0 \leq M - 5 \log h \leq -17.5$, where we find that it may be reasonably described by a Schechter function with $M^* = -20.29 \pm 0.02 + 5 \log h$, $\alpha = -0.70 \pm 0.05$, and $\phi^* = 0.019 \pm 0.001 \, h^3$ Mpc^{-3}. There appears to be an excess relative to the Schechter function at the faint end $M > -17.5$. The mean galaxy density for the range $-23.0 \leq M \leq -17.5$ is 0.029 ± 0.002 galaxies h^3 Mpc^{-3} out to a redshift of 60,000 km s^{-1}, and the run of cumulative density with redshift suggests that the density has converged within the LCRS survey volume. The measured galaxy luminosity density is $\rho_L = (1.4 \pm 0.1) \times 10^8 \, L_\odot \, h$ Mpc^{-3}, resulting in $\Omega = 0.2$ for a typical virial mass-to-light ratio of $300 \, h \, (M/L)_\odot$ and a rough isophotal-to-total light correction. We have also divided our sample by the cut [O II] $\lambda 3727$ equivalent width $W_\lambda \geq 5$ Å and have showed that the emission and nonemission galaxies so defined have significantly different luminosity functions, with emission galaxies dominating the faint end ($\alpha = -0.9 \pm 0.1$), nonemission galaxies dominating the bright end ($\alpha = -0.3 \pm 0.1$), and about equal numbers near the full sample M^*.

We then compared our results to those from the optically selected Stromlo-APM, CfA, and SSRS2 redshift surveys. Despite the fact that the Stromlo-APM survey has an $\alpha \approx -1$, and the LCRS has $\alpha = -0.7$, the shapes of two luminosity functions are remarkably similar, though they do differ in specific details. Moreover, our luminosity function normalization is consistent with that of Stromlo-APM; the CfA normalization is higher, but this may be biased by density inhomogeneities in its smaller and more local survey volume. Finally, our emission galaxy results confirm the picture seen in these previous surveys that the faint end of the luminosity function is dominated by late-type, blue galaxies which are presumably also gas rich and strong in [O II] $\lambda 3727$ emission.

Finally, two implications of our results may be made with respect to the faint galaxy counts and to galaxy evolution. First, our normalization of the luminosity function is a factor of 2 below the "high" normalization often adopted from the $b_J \approx 20$ APM galaxy counts in calculations used to match fainter galaxy count data. If our normalization is not an underestimate (e.g., because of surface brightness effects), then it implies that more evolution is required in the models, compared to using the high APM count normalization. Second, for the redshifts sampled in the Las Campanas survey, up to about $z = 0.2$ for galaxies brighter than M^*, our results do not indicate a significant change of average [O II] $\lambda 3727$ equivalent width with redshift. The star formation rate, as measured by [O II] $\lambda 3727$, has apparently not evolved rapidly over the volume sampled by the LCRS, unlike the large increases seen in the numbers of blue star-forming galaxies in smaller, deeper surveys at $z \gtrsim 0.3$.

In this paper we have used the Las Campanas Redshift Survey to provide an accurate determination of the local luminosity function for the largest galaxy sample thus analyzed. Our red R-band results are also complementary to previous results in blue photometric bands. In addition, we have begun to explore the luminosity function for galaxy samples divided by emission properties, and in future analyses we will examine galaxy samples defined by $b_J - R$ colors (which are available for our Southern galaxies from APM observations), and if possible, also by basic morphological information to be determined from our drift-scan images. The Las Campanas Redshift Survey should thereby provide a useful and large database of local galaxy properties, including luminosity, emission, color, and possibly morphological information, upon which to anchor models of faint galaxy counts and galaxy evolution at higher redshifts.

REFERENCES

Babul, A., & Rees, M. J. 1992, MNRAS, 255, 346
Binggeli, B., Sandage, A., & Tammann, G. A. 1988, AR&A, 26, 509
Broadhurst, T. J., Ellis, R. S., & Glazebrook, K. 1992, Nature, 355, 55
Broadhurst, T. J., Ellis, R. S., & Shanks, T. 1988, MNRAS, 235, 827
Carlberg, R., Yee, H. K. C., Ellingson, E., Abraham, R., Gravel, P., Morris, S., & Pritchet, C. J. 1996, ApJ, 462, 32
Colless, M. 1995, in Wide-Field Spectroscopy and the Distant Universe, Proc. 35th Herstmonceux Conf., ed. S. J. Maddox & A. Aragón-Salamanca (Singapore: World Scientific), 263
Colless, M., Ellis, R. S., Broadhurst, T. J., Taylor, K., & Peterson, B. A. 1993, MNRAS, 261, 19
Colless, M., Ellis, R. S., Taylor, K., & Hook, R. N. 1990, MNRAS, 244, 408

Colless, M., Schade, D., Broadhurst, T. J., & Ellis, R. S. 1994, MNRAS, 267, 1108
Cowie, L. L., Songaila, A., & Hu, E. M. 1991, Nature, 354, 460
da Costa, L. N., et al. 1994, ApJ, 424, L1
Davis, M., & Huchra, J. 1982, ApJ, 254, 437
Driver, S. P., Windhorst, R. A., & Griffiths, R. E. 1995a, ApJ, 453, 48
Driver, S. P., Windhorst, R. A., Ostrander, E. J., Keel, W. C., Griffiths, R. E., & Ratnatunga, K. U. 1995b, ApJ, 449, L23
Eales, S. 1993, ApJ, 404, 51
Efstathiou, G., Ellis, R. S., & Peterson, B. A. 1988, MNRAS, 232, 431 (EEP)
Felten, J. E. 1977, AJ, 82, 861
Ferguson, H. C., & McGaugh, S. S. 1995, ApJ, 440, 470
Geller, M. J., & Huchra, J. P. 1989, Science, 246, 897

Glazebrook, K., Ellis, R., Colless, M., Broadhurst, T., Allington-Smith, J., & Tanvir, N. 1995a, MNRAS, 273, 157
Glazebrook, K., Ellis, R., Santiago, B., & Griffiths, R. 1995b, MNRAS, 275, L19
Glazebrook, K., Peacock, J. A., Miller, L., & Collins, C. A. 1995c, MNRAS, 275, 169
Graham, J. A. 1981, PASP, 93, 29
———. 1982, PASP, 94, 244
Gronwall, C., & Koo, D. C. 1995, ApJ, 440, L1
Kennicutt, R. C. 1992, ApJ, 388, 310
Kirshner, R. P., Oemler, A., & Schechter, P. L. 1979, AJ, 84, 951
Kirshner, R. P., Oemler, A., Schechter, P. L., & Shectman, S. A. 1983, AJ, 88, 1285
Koo, D. C. 1995, in IAU Symp. 168, Examining the Big Bang and Diffuse Background Radiations, ed. M. Kafatos (Dordrecht: Kluwer), in press
Koo, D. C., Gronwall, C., & Bruzual, G. 1993, ApJ, 415, L21
Koo, D. C., & Kron, R. G. 1992, AR&A, 30, 613
Lilly, S. J., Tresse, L., Hammer, F., Crampton, D., & Le Fèvre, O. 1995, ApJ, 455, 105
Lin, H. 1995, Ph.D. thesis, Harvard Univ.
Lin, H., Kirshner, R. P., Shectman, S. A., Landy, S. D., Oemler, A., Tucker, D. L., & Schechter, P. L. 1996a, in preparation
Lin, H., Kirshner, R. P., Tucker, D. L., Shectman, S. A., Landy, S. D., Oemler, A., & Schechter, P. L. 1996b, in preparation
Lonsdale, C. J., & Chokshi, A. 1993, AJ, 105, 1333
Loveday, J., Peterson, B. A., Efstathiou, G., & Maddox, S. J. 1992, ApJ, 390, 338
Maddox, S. J., Sutherland, W. J., Efstathiou, G., & Loveday, J. 1990a, MNRAS, 243, 692
Maddox, S. J., Sutherland, W. J., Efstathiou, G., Loveday, J., & Peterson, B. A. 1990b, MNRAS, 247, 1P

Marzke, R. O., Geller, M. J., da Costa, L. N., & Huchra, J. P. 1995, AJ, 110, 477
Marzke, R. O., Geller, M. J., Huchra, J. P., & Corwin, H. G. 1994a, AJ, 108, 2
Marzke, R. O., Huchra, J. P., & Geller, M. J. 1994b, ApJ, 428, 43
McGaugh, S. S. 1994, Nature, 367, 538
Metcalfe, N., Fong, R., & Shanks, T. 1995a, MNRAS, 274, 769
Metcalfe, N., Shanks, T., Fong, R., & Jones, L. R. 1991, MNRAS, 249, 498
Metcalfe, N., Shanks, T., Fong, R., & Roche, N. 1995b, MNRAS, 273, 257
Rocca-Volmerange, B., & Guiderdoni, B. 1990, MNRAS, 247, 166
Sandage, A. 1973, ApJ, 183, 711
Sandage, A., Tammann, G. A., & Yahil, A. 1979, ApJ, 232, 352 (STY)
Schechter, P. 1976, ApJ, 203, 297
Shectman, S. A., Landy, S. D., Oemler, A., Tucker, D. L., Kirshner, R. P., Lin, H., & Schechter, P. L. 1995, in Wide-Field Spectroscopy and the Distant Universe, Proc. 35th Herstmonceux Conference, ed. S. J. Maddox & A. Aragón-Salamanca (Singapore: World Scientific), 98
———. 1996, in preparation
Shectman, S. A., Schechter, P. L., Oemler, A., Tucker, D., Kirshner, R. P., & Lin, H., 1992, in Clusters and Superclusters of Galaxies, ed. A. C. Fabian (Dordrecht: Kluwer), 351
Thuan, T. X., & Gunn, J. E. 1976, PASP, 88, 543
Tucker, D. L. 1994, Ph.D. thesis, Yale Univ.
Tucker, D. L., Oemler, A., Shectman, S. A., Landy, S. D., Kirshner, R. P., Lin, H., & Schechter, P. L. 1995, in Large Scale Structure in the Universe: Theoretical and Observational Aspects, Proc. 11th Potsdam Cosmology Workshop, in press
Yahil, A., Strauss, M. A., Davis, M., & Huchra, J. P. 1991, ApJ, 372, 380
Zucca, E., Pozzetti, L., & Zamorani, G. 1994, MNRAS, 269, 953

Note added in proof.—The difference noted here between the luminosity functions of emission and nonemission galaxies is similar to that found in preliminary analysis of the ESP redshift survey galaxies, e.g., Vettolani et al. (1994), IAU Symposium No. 161, 687.